Impact of HIV on Regionally Specific Brain Volumes in the HAART era: A Deformation- and Voxel-Based Morphometry Study

Ryan Sanford
Department of Biomedical Engineering
McGill University, Montreal, Canada

December 2015

A thesis submitted to McGill University in partial fulfillment of the requirements for the degree of Master of Engineering

Table of Contents

List of Figures

List of Tables

Acknowledgments

First, and foremost, I would like to thank my supervisor Dr. Louis Collins for his hard work and dedication, which allowed me to complete my Master's degree. He provided me with excellent advice, support and encouragement throughout my time as a Master's student. I look forward to continue learning under his supervision in my PhD studies.

I want to extend a special thank you to Dr. Beau M. Ances for providing me with copious amounts of well-organized patient data in a timely manner, as well as superb advice, encouragement and mentorship. Without his contributions, this whole project would not be possible. I would also like to thank Dr. Lesley K. Fellows for her valuable clinical insight, and support throughout the entire project.

I am further grateful to my colleagues who work in the Brain Imaging Center at the Montreal Neurological Institute. Ever since I arrived in May 2014, they have helped me every step of the way. I am especially grateful to Nicolas Guizard and Vladimir S. Fonov for answering all my image processing related questions with great detail.

Finally, I would like to thank the Natural Sciences and Engineering Research Council of Canada and McGill University for funding my studies.

Contribution of Authors

I am the first author in the manuscript included in this thesis. I was responsible for image analysis, which included all the image processing stages, quality control, statistical analysis, visualization, and interpretation of the results. The contributions of the co-authors included supervision of the project, data collection, and valuable insight and support over the course of the project. The following lists the co-authors and their respective contributions:

D. Louis Collins: Primary supervisor on this project. Provided valuable insight and advice in regards to the image processing steps.

Beau M. Ances: Neurologist at Washington University in St. Louis. Responsible for collecting all the patients' data and defining the scope of the project, and aided in the interpretation of the results.

Lesley K. Fellows: Neurologist at the Montreal Neurological Institute. Aided in defining the scope of the project and interpretation of the results.

Ana Lucia Fernandez Cruz: PhD student under the supervision of Dr. Fellows. She helped organize all the patients' clinical data.

Abstract

This thesis investigates the effect HIV has on the brain, as captured by magnetic resonance imaging (MRI), using advanced image processing methods: deformation-based morphometry (DBM) and voxel-based morphometry (VBM). It begins with a brief introduction to the human immunodeficiency virus (HIV), followed by the motivation and scientific objectives of the study. Chapter 2 provides an in-depth overview of HIV, its replication cycle, the mechanisms it uses to induce immune deficiency and HIV-associated neurocognitive disorders, and provides a short review of anti-retroviral therapy. Background information on magnetic resonance imaging, medical image processing, the MNI processing pipeline and statistical analysis are also outlined in Chapter 2. Chapter 3 takes the form a manuscript that provides evidence of regionally specific brain volume changes in a large sample of HIV+ patients on stable treatment with effective viral suppression. It should be noted that due to the nature of a Master's manuscript-based thesis, many key ideas and points will be repeated throughout this dissertation.

HIV is commonly associated with cognitive impairment, even when viral replication is effectively suppressed with highly active anti-retroviral therapy (HAART). Cognitive deficits may arise from brain injury directly related to the virus, to possible neurotoxic effects triggered at the time of initial infection, or to the many co-morbidities that may have a negative impact on brain function. Although several HIV-related MRI studies have provided vital information about the brain regions affected in HIV+ patients, the exact mechanisms underlying brain injury remain unclear.

The aims of the study in Chapter 3 were to characterize the nature and extent of regional brain volume differences between HIV+ individuals and a demographically similar HIV- group, and to assess whether measures of immune status, and current and past HIV infection severity are related to measures of regional brain volumes. We applied advanced neuroimaging analytic methods: DBM and VBM, to structural MRIs acquired in a large sample of HIV+ patients drawn from a United States infectious disease clinic, and a healthy HIV- comparison group drawn from the local community. We report regionally specific patterns of reduced subcortical volumes in the HIV+ sample, despite HAART yielding full viral suppression in the majority. Reduced white matter and subcortical volumes were related to nadir CD4 counts. However, current viral suppression and immune status did not relate to any regional brain volume changes. Our findings

argue for the importance of early treatment with HAART, before significant CD4 cell count decline, in protecting long term brain health.

Résumé

Cette thèse étudie l'effet du VIH sur le cerveau, comme capturé par imagerie par résonance magnétique (IRM), en utilisant des méthodes avancées de traitement d'image: morphométrie-déformation (DBM) et morphométrie voxel (VBM). Il commence par une brève introduction au virus de l'immunodéficience humaine (VIH), suivie par la motivation et les objectifs scientifiques de cette thèse. Le chapitre 2 donne un aperçu en profondeur du VIH, son cycle de réplication, les mécanismes qu'il utilise pour induire un déficit immunitaire et des troubles neurocognitifs associés au VIH, et fournit un bref examen de la thérapie anti-rétrovirale. Informations générales sur l'imagerie par résonance magnétique, traitement d'images médicales, le pipeline de traitement de l'INM et l'analyse statistique sont également décrites dans le chapitre 2. Le chapitre 3 prend la forme d'un manuscrit qui fournit des preuves de changements spécifiques à la région de volume du cerveau dans un grand échantillon de patients VIH + sur stable traitement avec une suppression virale efficace. Il convient de noter qu'en raison de la nature de la thèse sur la base de manuscrit d'une maîtrise, de nombreuses idées et les points clés seront répétées tout au long de cette thèse.

VIH est souvent associée à des troubles cognitifs, même lorsque la réplication virale est supprimée efficacement avec la thérapie anti-rétrovirale hautement active (HAART). Les déficits cognitifs peuvent découler de lésions cérébrales directement lié au virus, aux effets neurotoxiques possibles déclenchées au moment de l'infection initiale, ou pour les nombreuses co-morbidités qui pourraient avoir un impact négatif sur le fonctionnement du cerveau. Bien que plusieurs études IRM liées au VIH ont fourni des informations essentielles sur les régions du cerveau touchées dans les patients VIH +, les mécanismes exacts qui sous-tendent une lésion cérébrale restent floues.

Les objectifs de l'étude dans le chapitre 3 étaient de caractériser la nature et l'étendue des différences régionales de volume du cerveau entre les individus VIH + et un groupe VIH démographiquement similaire, et d'évaluer si des mesures de l'état immunitaire, et de gravité de l'infection actuelle et passée du VIH sont liés à mesures de volumes régionaux cérébraux. Nous avons appliqué des méthodes avancées d'analyse neuro-imagerie: DBM et VBM, à l'IRM structurelles acquises dans un large échantillon de patients VIH + tirée d'une maladie infectieuse clinique aux États-Unis, et un groupe de comparaison VIH saine tirée de la communauté locale. Nous rapportons les modèles spécifiques à la région de volumes sous-cortical réduits dans l'échantillon VIH +, malgré la multi thérapie cédant suppression virale complète dans la majorité. Substance blanche réduite et des volumes sous-cortical étaient liés à nadir de

CD4. Cependant, la suppression virale actuelle et l'état immunitaire ne se rapportent pas à des changements régionaux de volume du cerveau. Nos résultats plaident en faveur de l'importance d'un traitement précoce avec HAART, avant CD4 baisse significative de la numération cellulaire, dans la protection de la santé du cerveau à long terme.

Chapter 1: Introduction

HIV is a viral infection that attacks the immune system. Normally after seroconversion individuals experience flu-like symptoms, which is followed by a prolonged period without any symptoms (Levy, 1993). It is during this time that the infection interferes with the immune system. In particular, the virus infects and attacks immune cells, significantly reducing an individual's CD4+ T-cell counts, which is a vital component of the immune system (Levy, 1993). Without proper treatment, the virus will cripple the immune system such that the individual can no longer fight off life-threatening opportunistic infections and cancers (Lima et al., 2007). Before the introduction of HIV treatment, life expectancy among HIV+ patients was less than ten years after the initial infection diagnoses (Lima et al., 2007). In many cases, patients would discover they are HIV+ after contracting a rare opportunistic infection that would normally not affect individuals with working immune systems. The set of late symptoms associated with such infections is referred to as the acquired immunodeficiency syndrome (AIDS) (Levy, 1993). As outlined by the Centers for Disease Control and Prevention, patients are diagnosed with AIDS if their CD4+ T-cell counts reaches less than 200 cells/μL, the percentage of CD4+ T-cells out of total lymphocytes is less than 15%, or if one or more AIDS-defining illnesses are present (Selik et al., 2014). Examples of AIDS-defining illnesses include Kaposi's sarcoma, encephalitis and recurrent pneumonia (Selik et al., 2014). By 1996 researchers had developed different HIV treatment regimens, known as anti-retroviral therapy. However, each individual anti-retroviral drug could not effectively improve immune status on its own. To overcome this issue, researchers combined multiple anti-retroviral drugs, such that HIV replication was inhibited at multiple sites in the replication cycle. This multi-drug regimen is now known as highly active anti-retroviral therapy (HAART). In the HAART era, clinical and immune statuses have significantly improved, such that many HIV+ patients are living for more than twenty years after the initial infection (Ances, Orteg, Vaida, Heaps, & Paul, 2012). HAART has been very successful and many believe that an AIDS-free generation is within reach (Fauci & Folkers, 2012).

Some HIV+ patients also experience HIV-associated neurocognitive disorders (HAND), which significantly reduces the quality of life. Typically, severe forms of HAND occurred after years of infection, and was associated with low CD4+ cell counts and high viral loads (Ellis et al., 2011). It is believed that HAND is caused by the virus itself, as oppose to opportunistic infections. The virus enters the brain through the blood-brain barrier via infected immune cells, such as CD4+

T cells, macrophages and microglia, which is known as the "Trojan Horse" mechanism. (Kaul, Garden, & Lipton, 2001). Once in the brain, the virus and infected immune cells have a toxic effect on the neurons, leading to neurodegeneration, brain atrophy, and ultimately HAND.

1.1. Motivation

Prior to the advent of HAART, the prevalence of severe forms of HAND was estimated to be as high as 20-30% among those patients with advanced HIV infection and low CD4+ cell counts (McArthur et al., 1993). Since HAART was introduced, the incidence has decreased to as low as 10.5%, which has resulted in significant improvements in the quality of life among HIV+ patients (Kaul et al., 2001). However, the prevalence of mild to moderate forms of HAND appears to be increasing (Ances & Ellis, 2007; Heaton et al., 2011a). It has been reported that 30-50% of patients show minor cognitive deficits, despite stable HAART treatment and effective systemic viral suppression (Simioni et al., 2010). This illustrates the need to investigate brain volume changes in HIV+ patients with well-controlled infections, in an effort to uncover the precise mechanisms that may underlie brain injury and lead to cognitive deficits.

HIV-related structural MRI studies have provided key evidence concerning the topography of brain changes due to HIV (Holt, Kraft-Terry, & Chang, 2012; Masters & Ances, 2014). However, the reported patterns of atrophy across studies are inconsistent and the literature has yet to produce a clear consensus of the mechanisms that may underlie brain injury. Inconsistencies across studies reflect several factors, including differences in the degree of infection and impairment severity in the HIV+ cohort, poorly matched HIV- comparison group and small sample sizes. In addition, the MRI processing methods utilized in several studies do not provide sufficient statistical power to detect meaningful brain volume changes, and they suffer from significant technical limitations.

In the study presented in Chapter 3, we propose to overcome the limitations encountered in previous studies by reporting on a large sample of HIV+ patients drawn and a demographically similar HIV- community-based comparison group. Nearly all of the HIV+ subjects were on stable HAART treatment, and the majority had full viral suppression. We aim to characterize the nature and extent of regional brain volume differences between HIV+ and HIV- individuals, and to examine the correlation between measures of immune status, and current and past HIV infection severity, with measures of regional brain volume. We applied advanced MRI processing techniques with complementary strengths to assess brain structure volumes: DBM and VBM, to

provide evidence of the regionally specific effects the infection has on the brain. Our findings should provide detailed illustrations of the regional brain volumes affected by HIV in HAART-treated HIV+ patients, and offer valuable insight into the potential mechanisms that may underlie brain injury and lead to cognitive impairment.

1.2. Scientific Objectives

- Observe the effect HIV has on the regional brain volumes in a large sample of HIV+ patients, on stable HAART treatment and effective viral suppression, compared to a demographically similar healthy control group.
- Investigate the relationship between measures of immune status, and current and past infection severity with regional brain volume changes.
- Utilize a suite of advanced medical image processing techniques: DBM and VBM, to provide accurate illustrations of where brain volume changes are associated with HIV, and how these regions are related to HIV-related clinical measures in the HAART era.

Chapter 2: Background

The following section provides an in-depth review into HIV, its replication cycle, the mechanisms it uses to induce immune deficiency, brain injury and cognitive impairment, and provides an overview of current HIV anti-retroviral treatment. It also provides a thorough review of magnetic resonance imaging and medical image processing techniques. Together, these methods were used to investigate and characterize the impact HIV has on the brain, as outlined in the manuscript in Chapter 3.

2.1. Human Immunodeficiency Virus

Acquired immunodeficiency syndrome (AIDS) is an infection that attacks the immune system. With a weak immune response, individuals with AIDS cannot fight opportunistic infections and cancers and these may become life-threatening (Lima et al., 2007). Thus, before treatment was available the life expectancy among AIDS patients was less than ten years after the initial infection diagnoses (Lima et al., 2007).

The first case of AIDS was reported in 1981, where five males had rare infections that indicated their immune systems were not working properly (Merson, 2006). By 1983 it was believed that AIDS was caused by a virus from the *Retroviridae* family, which was a type of enveloped virus that replicates in a host cell through a reverse transcriptase enzyme (Levy, 1993). Barre-Sinoussi *et al.,* (Barre-Sinoussi et al., 1983), investigated a reverse transcriptase-containing virus that was recovered from an AIDS patient with persistent lymphadenopathy syndrome. They identified it as a human T-cell leukemia virus (HTLV), a known retrovirus that caused cancer and nerve demyelination (Levy, 1993). However, HTLV did not explain the immune deficiency that was common in all AIDS patients (Levy, 1993). Further studies conducted in 1983 led to the discovery of three prototype viruses, all of which were believed to cause AIDS: HTLV-III, lymphadenopathy-associated virus and AIDS-associated retrovirus. All the viruses were part of the *Retroviridae* family, had the same properties, proteins and genomes, and were distinct from those of HTLV. Therefore, in 1986 the International Committee on Taxonomy of Viruses recommended giving the AIDS virus a separate name, the human immunodeficiency virus (HIV) (Levy, 1993).

2.1.1. Human Immunodeficiency Virus Structure

The structure of HIV was revealed through electron microscopy. It was spherical in shape and contained a cone-shaped core that was referred to as the capsid. The capsid was composed of viral proteins, and contained two copies of single-stranded RNA, reverse transcriptase, nucleocapsid proteins and other viral enzymes (Levy, 1993). Surrounding the capsid was the phospholipid bilayer, known as the viral envelope. Embedded in the viral envelope were 72 copies of complex HIV proteins. These proteins consisted of three glycoprotein (gp) 120 and gp41 molecules. This complex protein structure enabled the virus to attach itself and fuse with target cells (Levy, 1993). An example of the HIV structure is displayed in Figure 1.

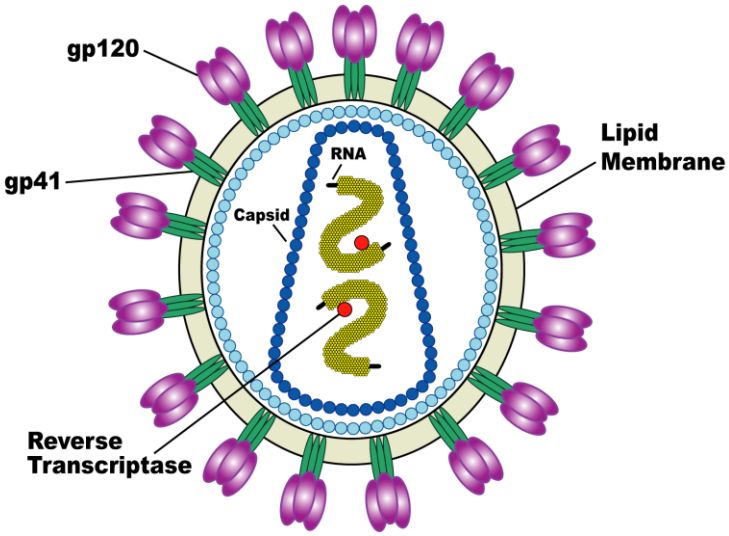

Figure 1: A typical HIV virion consists of a surrounding lipid membrane known as the viral envelope. The viral envelope is composed of viral proteins gp120 and gp141. Inside the HIV cell is the capsid, which encapsulates two copies of RNA, reverse transcriptase, nucleocapsid proteins and other viral enzymes. Adapted from Yale Scientific (Wang, 2014).

2.1.2. HIV Pathogenesis and Replication Cycle

HIV infects a variety of immune cells such as CD4+ T helper cells, macrophages and microglial cells, which explains the weakened immune response in HIV/AIDS individuals (Levy, 1993). The viral entry into host cells is mediated through the interaction of the HIV viral envelope glycoproteins and the CD4 receptors, which are commonly found on immune cells (Levy, 1993). In particular, there is an interaction between gp120 and the CD4 receptor. This leads to a conformational change in gp120 that allows it to then interact with the β-chemokine receptor CCR5 on the immune cell. The gp41 molecules are then inserted into the cellular membrane of the host cell, which enables the viral and cellular membranes to fuse together (Levy, 1993). Once the cellular membranes have fused, the two single-stranded viral RNA, reverse transcriptase and other

viral enzymes are injected into the cell. The reverse transcriptase is responsible for transcribing the single-stranded viral RNA into a double-stranded viral DNA. The viral DNA is then integrated with the host cell's DNA via the viral enzyme integrase (Levy, 1993). The integrated viral DNA may lie dormant in the host cell for extended periods of time. This is why HIV is considered a *lentivirus* because it has a long incubation period (Levy, 1993). In order to begin producing new HIV viruses, there must be specific transcription factors present such as NF-κB. Ironically, NF-κB is upregulated in CD4+ T helper cells when they are activated, which means the CD4+ cells that are fighting off the viral infection are most likely to produce more HIV virions, and be killed (Levy, 1993). When the transcription factors are present, the integrated viral DNA is transcribed into mRNA, spliced and transported to the cytoplasm from the nucleus. In the cytoplasm, the spliced mRNAs are translated to produce HIV regulatory proteins *tat* and *Rev*, which have a strong influence on viral production (Levy, 1993). These regulatory proteins will begin to accumulate in the nucleus and enable newly formed mRNA to leave the nucleus unspliced. These full-length mRNA strands are the actual HIV genome that will be inserted into a newly formed HIV virus. In addition, they will produce the structural proteins *Gag* and *Env* (Levy, 1993). The *Env* protein is responsible for producing the gp120 and gp41 molecules and transporting them to the host cell's plasma membrane, where they will be a part of the viral envelope in the new virus. At this point, an immature HIV virus containing the *Gag* protein and two full-length mRNAs will bud off the host cell (Levy, 1993). However, an immature virus cannot infect other cells because it does not have the necessary viral enzymes. In order to become a mature HIV virus, the *Gag* protein, with the help of a viral protease, will bind to the viral RNA to produce the surrounding capsid, reverse transcriptase, nucleocapsid proteins and other viral enzymes (Levy, 1993). Once this is complete, the HIV virus is considered mature and has the ability to infect other immune cells and repeat the entire viral replication process (Levy, 1993). Figure 2 provides an overview of the HIV replication cycle.

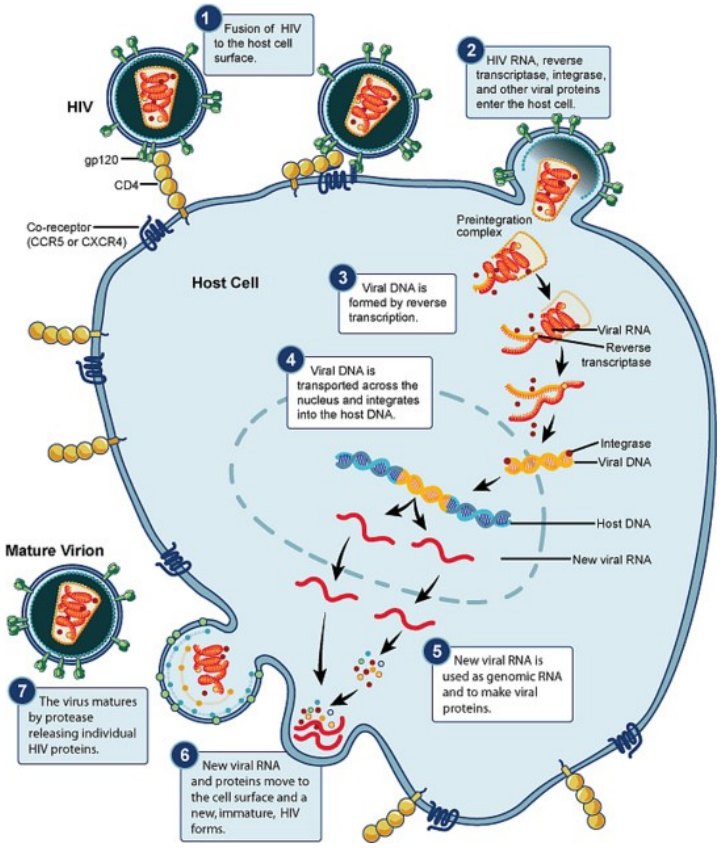

Figure 2: HIV viral replication cycle. The gp120 protein, attached to the viral envelope, will bind to a CD4 receptor on the host cell, resulting in cell fusion. The HIV RNA will be injected into the host cell, reverse transcribed into viral DNA, and integrated into the host cell's DNA. New viral RNA will be transcribed with new viral proteins. The resulting viral RNA and proteins will bud off of the host cell, creating a new HIV virion. Courtesy: National Institute of Allergy and Infectious Diseases (HIV Virus Replication Cycle, 2010).

2.1.3. HIV-Induced Cell Death and Immune Deficiency

Although it is widely known that patients with HIV/AIDS have a characteristic loss of immune function and significant depletion of CD4+ T helper cells, the cause still remains unclear. Many studies have investigated HIV-induced cell death, where direct toxic effects from the virus and the associated viral proteins on immune cells could, in part, explain the immune deficiency and characteristic CD4+ T helper cell loss. In particular, one study infected cells with HIV and doubled the production of gp120. As a result, the authors reported increased cell death in the infected cells that had more gp120 molecules (Stevenson, Meier, Mann, Chapman, & Wasiak, 1988). It was also reported that HIV may have a peptide that acts like a super-antigen and attaches to CD4+ T helper cells, which will induce programmed cell death via apoptosis (Coffin, 1992). These studies suggested that HIV-induced cell death results in significant CD4+ T helper cell loss, which ultimately leads to immune deficiency. However, several other studies have observed immune deficiency before significant CD4+ T helper cell depletion, suggesting that other possible

viral mechanisms could cause a loss of immune function (Levy, 1993). It was reported that the virus could infect or suppress the production of the early precursors of CD4+ cells and reduce the quantity of fresh lymphocytes added from the bone marrow to the peripheral blood (Folks et al., 1988). In addition, the HIV *tat* gene expressed in infected cells might reduce the responses of CD4+ cells to recall antigens, which will contribute to the immune deficiency (Viscidi, Mayur, Lederman, & Frankel, 1989). One mechanism known as the *bystander effect*, where immune cells destroy uninfected CD4+ cells when HIV and viral proteins are present (Lanzavecchia, Roosnek, Gregory, Berman, & Abrignani, 1988), has been investigated as a possible cause of immune deficiency. Another theory has suggested that viral envelope proteins could have an immunosuppressive effect on the CD4+ T helper cells (Chanh, Kennedy, & Kanda, 1988). The interplay of all these processes and mechanisms could collectively contribute to the weakening of the immune response and significant CD4+ T helper cell depletion in HIV/AIDS patients (Levy, 1993).

2.1.4. HIV Treatment: Anti-retroviral therapy

In 1985 the first effective HIV anti-retroviral treatment was developed. It was a nucleoside reverse transcriptase inhibitor (NRTI), referred to as zidovudine (AZT) (Mitsuya et al., 1985). AZT worked by inhibiting the reverse transcriptase enzyme, which was responsible for transcribing the single-stranded viral RNA into double-stranded viral DNA (Levy, 1993). The NRTI would prevent nucleosides from being added to the viral DNA (Mitsuya et al., 1985). Since viral DNA formation was inhibited, it would not be able to integrate itself into the host cell's DNA and ultimately prevented HIV replication (Mitsuya et al., 1985). Based on results from clinical trials, AZT significantly reduced viral replication and led to improved clinical and immune statuses (Wright, 1986). In 1987 AZT was approved for public use by the United States Food and Drug Administration (Molotsky, 1987). Although the clinical trials produced promising results, AZT could only slow down HIV replication but not stop it entirely. In addition, HIV became AZT-resistance after continuous use (Moore & Chaisson, 1996). Thus, AZT was not a viable long term treatment option because it was unable to suppress viral replication for longer periods of time and ultimately patients still died (Moore & Chaisson, 1996).

2.1.5. Highly Active Anti-retroviral Therapy

In 1996 a new class of anti-retrovirals, namely protease inhibitors, was created. The protease inhibitor would inhibit the viral enzyme protease from producing the capsid, reverse

transcriptase and nucleocapsid proteins, which prevented mature HIV viruses from forming and infecting other cells (Markowitz et al., 1995). Investigators then proposed a three-drug HIV therapy that included one protease inhibitor and two NRTIs (Gulick et al., 1997; Hammer et al., 1997). This combination of drugs resulted in significantly decreased HIV viral loads of less than 500 copies per millimeter for as long as one year, and elevated CD4+ cell counts (Gulick et al., 1997; Markowitz et al., 1995). This three-drug therapy was quickly integrated into clinical practice and showed significant improvements in clinical and immune statuses, with a 60-80% decline in rates of AIDS, death and hospitalizations (Moore & Chaisson, 1996). The three-drug therapy is now referred to as highly active anti-retroviral therapy (HAART), or combination anti-retroviral therapy, and has been estimated to have saved more than 700,000 lives, globally, in 2010 (Fauci & Folkers, 2012).

Currently, there are five classes of anti-retroviral drugs, including NRTIs and protease inhibitors, which can be used in combination to treat HIV and improve immune function. Each of the five classes are focused on inhibiting a certain phase of the viral replication cycle. Entry or fusion inhibitors will obstruct the binding, fusion and entry of the virus into the host cell. It does so by blocking the CCR5 receptor or by inhibiting the gp41 activity (Bai et al., 2013; Lieberman-Blum, Fung, & Bandres, 2008). Non-nucleoside reverse transcriptase inhibitors are similar to NRTIs except, instead of preventing nucleosides from being added to the double-stranded viral DNA, it inhibits the reverse transcriptase activity by binding to the allosteric site found on the enzyme (Das & Arnold, 2013). Integrase inhibitors will inhibit the viral enzyme integrase, which is responsible for integrating the double-stranded viral DNA into the host cell's DNA (Metifiot, Marchand, & Pommier, 2013). A typical HAART regimen consists of two NRTIs and one non-nucleoside reverse transcriptase inhibitor, protease inhibitor, fusion inhibitor, or integrase inhibitor. The diagram in Figure 3 illustrates where each anti-retroviral drug acts in the HIV viral replication cycle.

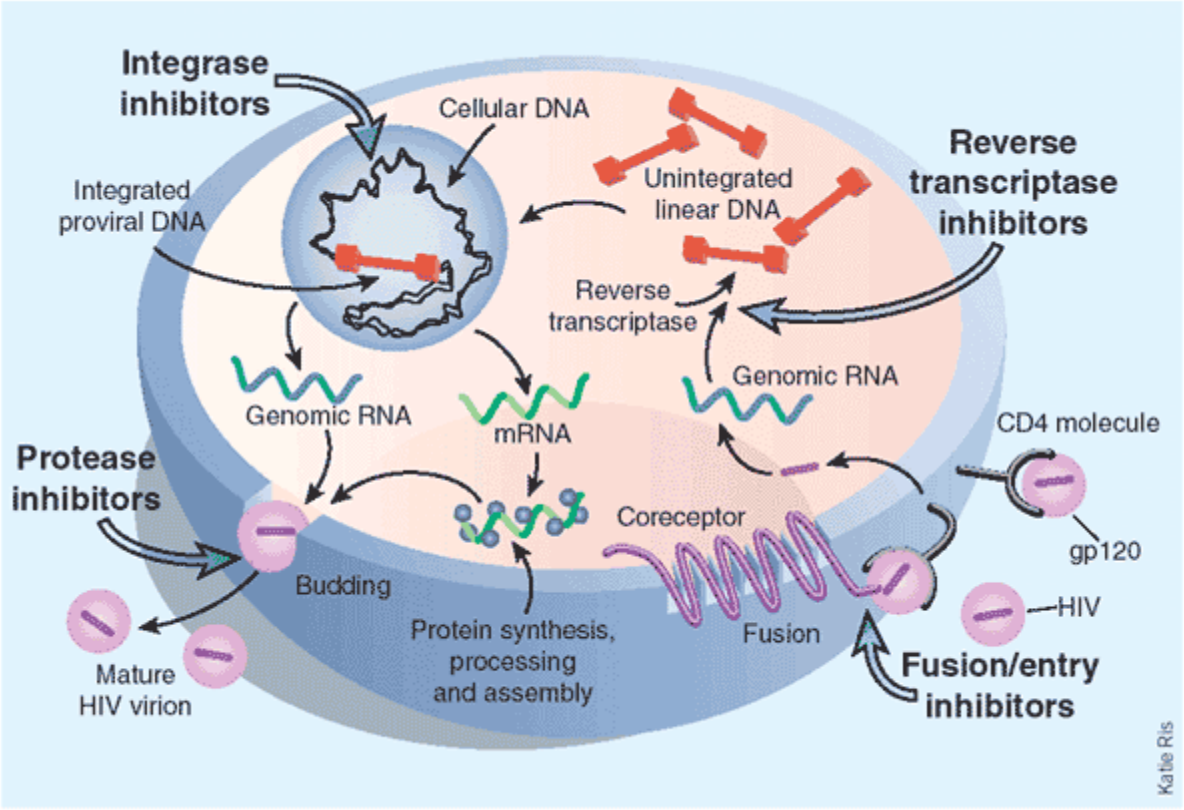

Figure 3: Each class of anti-retroviral drug will inhibit a different part of the HIV replication cycle. Highly active anti-retroviral therapy consists of combining multiple anti-retroviral drugs from different classes to prevent HIV replication. Courtesy: The Biology Project ("The replication cycle of HIV," 2000).

2.1.6. HIV-Associated Neurocognitive Disorders

In addition to immune deficiency, HIV/AIDS patients experienced HIV-induced neurocognitive disorders (HAND) after the initial infection (Kaul et al., 2001). Severe forms of HAND usually occurred after years of infection, and was associated with low CD4+ cell counts and high viral loads (Ellis et al., 2011). In some cases it was the first sign of the onset of AIDS. It was even believed that HIV-associated dementia was the most common cause of dementia worldwide among people aged 40 years or less (Kaul et al., 2001).

The principal pathway of HIV into the brain is believed to be through infected microglia and macrophages that have successfully passed through the blood-brain barrier (Kaul et al., 2001). Once in the brain, the infected macrophages and microglia cells release the viral envelope protein gp120, cytokines and chemokines, which activate uninfected macrophages and microglia. These activated and infected cells then release potentially neurotoxic substances such as quinolinic acid, glutamate, arachidonic acid and free radicals (Kaul et al., 2001). These substances induce neuronal injury, dendritic and synaptic damage, and apoptosis, all of which could lead to cognitive

impairment (Kaul et al., 2001). Astrocytes in the brain have also been reported to play a role in HAND. When astrocytes were exposed to arachidonic acid, released by macrophages and microglia, it resulted in impaired glutamate uptake, increased glutamate release, and induction of nitric oxide synthase, leading to release of potentially neurotoxic nitric oxide (Kaul et al., 2001). Multiple researchers believe that neuronal injury could be caused by viral proteins such as *tat,* gp120 and gp41, which may have a direct toxic effect on the neurons (Kaul et al., 2001). Experiments have shown that the viral envelope proteins were toxic in neuronal cultures (Meucci et al., 1998) and neuroblastoma cell lines (Hesselgesser et al., 1997). However, other reports have concluded that neuronal injury may be caused by an indirect effect from the virus, such as the bystander effect hypothesis (Kaul et al., 2001). Experiments have shown that for HIV and gp120 to be neurotoxic to cerebrocortical neurons, the presence of macrophages/microglia were required (Kaul & Lipton, 1999; Lipton & Gendelman, 1995). It was also shown that HIV infected or gp120-stimulated mononuclear phagocytes released neurotoxins that stimulated N-methyl-D-aspartate receptors resulting in neuronal damage (Kaul et al., 2001). Although direct and indirect toxic effects currently have data to support both theories, neurotoxicity via the indirect form seems to have the most support (Kaul et al., 2001).

2.2. Magnetic Resonance Imaging

Magnetic resonance imaging is a medical imaging technique used to investigate the anatomy of the human body. It is non-invasive and does not expose the patient to harmful radiation. This makes it a popular choice to use for diagnosis and staging of diseases. Figure 4 shows a typical MR head scan from one patient.

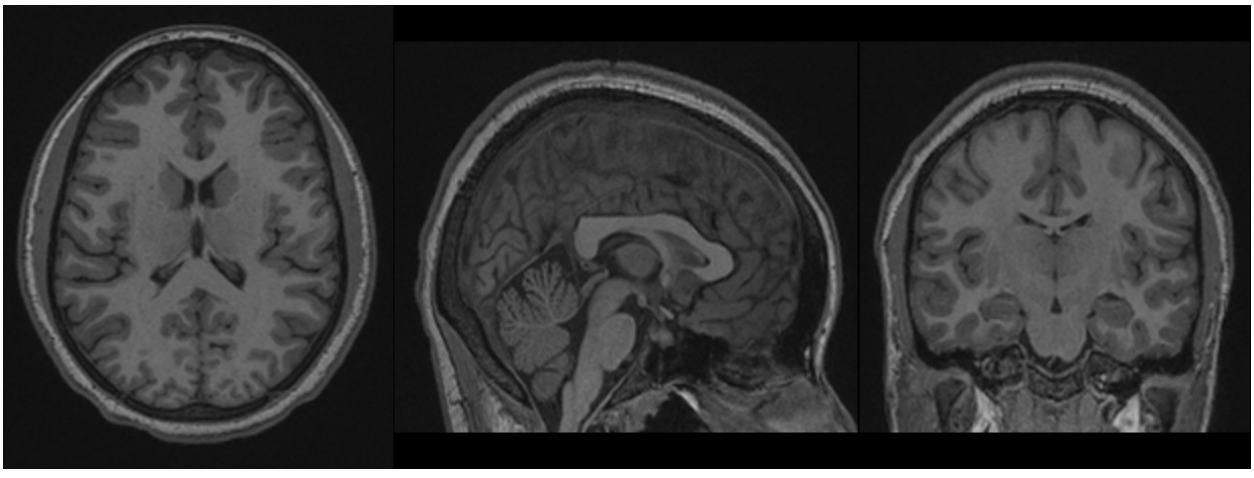

Figure 4: Example of a typical MR head scan.

The signal used to create the MRI originates from hydrogen atoms (protons) that are found in tissues containing water molecules. Each hydrogen atom can be in one of two spin states, ±½, which defines its magnetic moment. The hydrogen atoms, at any given moment in time, are randomly spinning around their own axis with the magnetic moment pointing in random directions. When a strong magnetic field is applied, such as the one produced by the MR scanner, the magnetic moments of a portion of the hydrogen atoms in the entire body will align with the magnetic field, which is defined as the *z*-axis. At this point, however, no signal has been created yet. In order to create the signal, a radio frequency (RF) pulse is applied perpendicular to the strong magnetic field. This will cause the magnetic moments of groups of hydrogen atoms to tip into the *xy*-plane. The hydrogen atoms are now considered to be precessing around the *z*-axis, in phase with the magnetic moments pointing along the *xy*-plane. When the RF pulse is turned off, the group of hydrogen atoms will return to their normal equilibrium state by realigning their magnetic moments with the magnetic field in the *z*-axis over a short period of time. The magnetic moments will also dephase in the *xy*-plane due to interactions between the hydrogen atoms and the surrounding chemical environment. It is during this time in which the MR signal is created. While recovering back to their equilibrium state or dephasing in the *xy*-plane, each precessing hydrogen atom will emit a radio frequency signal that is captured by receiving coils. This radio frequency signal is ultimately the signal that produces the MRI. In particular, the RF signal obtained from the hydrogen atoms are captured in two time constants T_1 and T_2. The T_1 time constant, or spin-lattice time, is the rate at which a hydrogen atom recovers back to its equilibrium state. It is calculated as the time it takes for a hydrogen atom to return to approximately 63% of its equilibrium state, as it realigns with the magnetic field in the *z*-axis. Equation 1 characterizes the recovery as an exponential function, where M_z is the magnetization in the *z*-axis at time *t* and $M_{z,eq}$ is the magnetization in the *z*-axis at equilibrium. This equation assumes M_z is initially 0 at time t=0.

$$M_z = M_{z,eq}(1 - e^{-t/T1})$$

Equation 1: Spin-lattice relaxation.

Meanwhile, the T_2 time constant, or spin-spin relaxation time, is the rate at which the net magnetization in the *xy-p*lane decays to zero. It is calculated as the time it takes for the net magnetization in the *xy*-plane to decay to approximately 37% of its original value. Equation 2

characterizes the decay as an exponential function, where M_{xy} is the magnetization in the *xy*-plane at time *t*.

$$M_{xy} = M_{xy}(0)e^{-t/T2}$$

Equation 2: Spin-spin relaxation.

The T_1 and T_2 time constants will vary depending on the local chemical environment surrounding the hydrogen atoms. This is why MRI results in excellent soft tissue contrast because hydrogen atoms belonging to gray matter, white matter, or cerebrospinal fluid (CSF) will each have different T_1 and T_2 time constants. By adjusting the pulse sequences time of echo (TE) and time of repetition (TR) the scanner can adjust the amount T_1 and T_2 contributions captured by the receiving coils, which gives rise to different MRI images, such as T_1-, T_2-, T_2^*- and proton density (PD)-weighted images. T_1-weighted images are produced by de-emphasizing the T_2 contributions, which is normally achieved by using short TR (300-600 ms) and short TE (10-15 ms). These images are useful for studying the cerebral cortex because the T_1 relaxation times for gray and white matter are significantly different, resulting in good tissue contrast. Meanwhile, T_2-weighted images are produced by de-emphasizing the T_1 contributions. This is typically done with long TR (2000-6000ms) and long TE (100-150ms). T_2-weighted images are useful for revealing white matter lesions, such as those found in the brains of multiple sclerosis patients due to high levels of oedema. In practice, however, the T_2 time constant is much faster than predicted in Equation 2. This observed rate of transverse magnetization decay is denoted as T_2*. Typically, the TR and TE can be adjusted to take advantage of the T_2* decay time to accentuate local homogeneity effects, which can be used to detect hemorrhage and calcifications. Finally, PD-weighted images are produced by minimizing the T_1 and T_2 contribution differences. This can be achieved with long TR (2000-6000ms) and short TE (10-15ms). Similar to T_1-weighted images, PD-weighted images produce good tissue contrast between gray and white matter. Examples of T_1- and T_2-weighted images of the brain are shown in Figure 5.

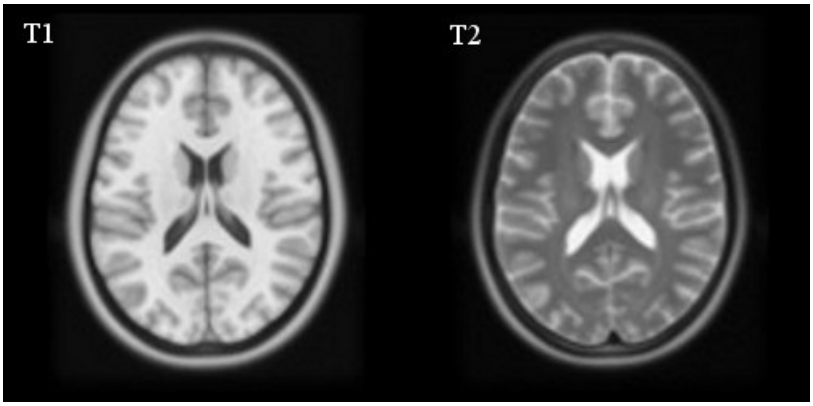

Figure 5: Examples of T1- and T2-weighted MR scans.

All MR scanners consist of three gradient coils, one for each direction in space, that are responsible for varying the local magnetic field to permit spatial encoding. The gradient coils will vary the magnetic field across the body such that hydrogen atoms in different spatial locations emit RF signals with a slightly different frequency and phase. These signals are mapped onto a *k*-space, which is where the raw data is stored before reconstruction, depending on the frequency and phase. Thus, each point of the *k*-space corresponds to a unique RF signal originating from a known spatial location, as defined by the gradients. The inverse Fourier transform is then applied to the *k*-space to reconstruct the final image.

2.3. Image Processing

Typically, the voxel size for a T_1-weighted MR image is 1x1x1 mm^3, which allows for each tissue type to easily distinguishable from one another. However, before the raw MR images can be used in any neuro-anatomical study, they must be processed. Most MR image processing methods consists of a series of steps that combine to extract information that can be effectively analyzed with statistical models. These steps can be performed manually, semi- or fully-automatically. Manual or semi-automatic techniques require human intervention, which makes them labour intensive and subject to inter- and intra-rater variability. In contrast, fully-automatic methods have the advantage of processing large amounts of data with no human intervention. In addition, fully-automatic programs have high reproducibility because they are not susceptible to inter- and intra-rater variability.

When MR scans are being processed important information, such as global volume measurements, local volumetric information about specific structures and information at the voxel level, can be extracted. With the resulting information, various statistical models and methods can

be applied to identify structural abnormalities and brain volume differences between groups or changes over time. The following sections summarize two key steps in every image processing pipeline: image registration and segmentation. Sections 2.3.3-2.3.5 provides an overview of three image processing methods: region-of-interest (ROI)-analysis, DBM and VBM, which have been widely utilized in several structural MRI studies.

2.3.1. Image Registration

A vital step for all medical image processing techniques is image registration, where the goal is to adequately align corresponding brain structures to a common reference frame. This is very important because it helps to compare data, classify data and detect statistically significant patterns across the data (Klein et al., 2009).

Image registration techniques can be classified into two broad categories: linear and non-linear. Linear registration aligns two images by finding an optimal 6, 9 or 12 parameter affine transformation that maximizes some objective function. Popular objective function choices for linear registration are cross-correlation, mutual information and sum of squared differences (Pluim, Maintz, & Viergever, 2000). These objective functions use the intensity information to measure the similarity, on voxel-wise basis, between the two images. In theory, when the similarity measure between two MR head scans are maximized, corresponding brain structures should be aligned. Linear registration is useful for transforming MR scans into a common anatomical space and it is normally one of the first steps for image processing. However, it has been well-established that linear registration does not adequately align brain structures due to the inter-individual variability of the brain (Klein et al., 2009). Thus, non-linear registration techniques have been developed to provide stronger brain structure alignment and account for inter-individual variability.

Typical non-linear registration procedures involves finding the optimal non-linear transformation that maps each voxel of the subject's MRI to its corresponding location on a brain template (Collins, Holmes, Peters, & Evans, 1995). This process will essentially warp the patient's MR scan such that all regions of the brain are optimally aligned with the corresponding region in the brain template (Collins et al., 1995). The brain template can be based on an average brain created from many adult brains, such as the atlases provided by the Montreal Neurological Institute (http://www.bic.mni.mcgill.ca/ServicesAtlases/HomePage), or created from the subjects within the study. Choosing an average brain atlas will avoid bias towards particular brain geometry, but

may not be ideal for diseased cohorts. In contrast, creating a brain template from subjects within a study will result strong registration quality, but may introduce bias to particular anatomical geometries. An example of a non-linear registration strategy is displayed in Figure 6, where a particular node x_1 is warped to $D(x_1)$ by maximizing some objective function. Similar to linear registration, the objective functions can use the intensity information to measure the similarity. However, other objective functions have been used successfully such as the Jensen-Rényi divergence (Chiang et al., 2007) and residual squared differences (Ashburner & Friston, 1999). The optimal non-linear transformation that warps a MR scan to match a common template can be represented as a deformation field. As seen in Figure 6, the deformation field is viewed as a collection "arrows" at every grid point. Each point on the grid can be viewed as a deformation tensor field that encodes the position, size and shape of the patient's MR scan relative to the brain template (Lepore et al., 2008). The full deformation tensor contains useful information about the volume and shape of brain structures, and is the basis for deformation-based morphometry. However, as discussed in section 2.3.4, different mathematical operations must be applied to deformation field to recover the volumetric and shape information.

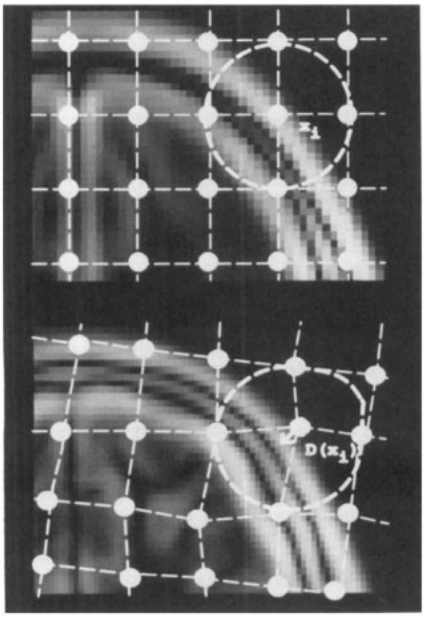

Figure 6: Non-linear registration strategy. Mapping the node x_1 to $D(x_1)$ by finding the optimal non-linear transformation (Collins et al., 1995).

2.3.2. Brain Segmentation and Tissue Classification

The purpose of brain segmentation and tissue classification is to label each unique structure and tissue type in the brain, respectively. With a fully-segmented brain, morphological

information, such as volume and shape, can be captured and used for future statistical analysis. Segmentation of MR scans have played a key role in many studies in recent years. It provides researchers with useful information about the brain and how a neurological disease could affect it.

Several brain segmentation methods have previously been developed (Brummer, 1992; Kundu, 1990; W. M. Wells, E. L. Grimson, R. Kikinis, & F. A. Jolesz, 1996a). These methods took advantage of the unique intensity information provided by the MR data to segment the brain. Although the intensity information was useful, the resulting segmentations were inaccurate due to noise, intensity nonuniformity and poor image contrast present in the MR data (Fischl et al., 2002). In addition, even if the MR images were preprocessed to reduce noise and artifacts, there was no guarantee that the intensities of each structure and tissue type were unique. Consequently, brain segmentation accuracy would not be sufficient enough to perform meaningful statistical analysis.

To increase the brain segmentation accuracy and robustness, algorithms have been developed to not only use the intensity information but also incorporate spatial and contextual information (Zhang, Brady, & Smith, 2001). The structures of the human brain occur in a characteristic spatial pattern that is known prior to receiving any MR data. For example, the hippocampus and amygdala are both gray matter structures with almost identical intensities, which makes them difficult to differentiate. Rather than relying on the intensities, anatomists utilize spatial information, where they realize the amygdala is always anterior and superior to the hippocampus (Fischl et al., 2002). It was also well-known that the tissues in the brain always appear in clusters. For example, gray matter voxels, in general, will be surrounded by more gray matter voxels. Therefore, by incorporating spatial and contextual information, along with the intensity information, the brain segmentation accuracy and robustness increases. Spatial information are commonly encoded using Markov Random Fields or Conditional Random Fields (Fischl et al., 2002). These are graphical models compute the probability of each voxel label given the current estimate of the labels in a finite number of neighboring voxels. By tuning various hyper-parameters, these graphical models will force voxel labels to be similar, or dissimilar, to neighboring voxels.

Other segmentation techniques have been developed to take advantage of tissue probability maps and manually-segmented structural atlases. In particular, Collins *et al.*, (Collins et al., 1995), developed a brain segmentation strategy that uses labels from a manually-segmented structural atlas to segment a new MR scan. Thus, the authors posed the segmentation problem as a

registration problem (Collins et al., 1995). They developed a general, iterative, hierarchical non-linear registration procedure that maps corresponding intensity-based features between a patient's MR scan and the manually-segmented structural atlas. Once completed, the labels from the structural atlas are mapped back through the non-linear transformation to segment the structures in the patient's MR scan (Collins et al., 1995).

Tissue probability maps have also been employed to train neural networks to classify the tissues in the brain. In particular, Zijdenbos *et al.*, (Zijdenbos, Forghani, & Evans, 2002), developed a method that samples 1000 randomly chosen points from the tissue probability maps. These randomly chosen points are then used to train an artificial neural network classifier based on the tissue signal intensity characteristics in the MR scan to be classified (Zijdenbos et al., 2002).

2.3.3. Regions of interest analysis

A popular method to assess structural brain volume changes across populations from MR scans is the region-of-interest (ROI)-based volumetric method. Many neuro-anatomical studies have used traditional ROI-based analysis, where the volumes of particular anatomical structures are compared across study groups or correlated against disease-related clinical measures (Ances et al., 2012; Camicioli et al., 2003; Cohen et al., 2010; Csernansky et al., 2005; Fischl et al., 2002; Jernigan et al., 2011). However, these methods typically require prior hypotheses about where volumetric differences will be found, particularly when applied in small samples (Chung et al., 2001). These hypothesis-driven experiments cannot discover unpredicted volume differences, and when statistical power is low, null findings may not provide additional information. The results of ROI-based studies are also sensitive to the employed brain structure segmentation method, speaking to the considerable analytic challenges in the rapidly evolving neuroimaging field (Dewey et al., 2010). Alternative approaches have been developed to detect structural abnormalities that do not depend on *a priori* anatomical hypotheses (Ashburner & Friston, 2000). These include deformation-based morphometry and voxel-based morphometry. These techniques search the whole brain simultaneously at voxel level (i.e. 1 x 1 x 1 mm^3) for between-group differences, and can also test for correlations with explanatory variables at the same high spatial resolution.

2.3.4. Deformation-based morphometry

Deformation-based morphometry (DBM) is an alternative approach to identify global or gross brain volume changes from MR scans. It characterizes volume and shape differences across

different populations, relative to some digital brain model, at the macroscopic scale (Ashburner et al., 1998). To capture these volume and shape changes, DBM heavily relies on the deformation field that is generated by non-linearly registering the patient's MR scan with a brain template. The resulting deformation field contains useful information about local volume and shape of the patient's brain. To recover this information, the Jacobian determinant, also known as the volume expansion factor, is applied to the deformation field (Thompson & Toga, 1999). The Jacobian, in theory, describes the amount of stretching, rotating and shearing that the non-linear transformation has imposed on MR scan (Thompson & Toga, 1999). When the determinant is applied to the Jacobian, local brain growth or shrinkage, relative to the brain template, is revealed. In particular, if the Jacobian determinant is greater than one it implies volumetric expansion, while a Jacobian determinant less than one is associated with local shrinkage. A Jacobian determinant equal to one suggests that there is no volume change. When many subjects' scans are aligned to a common anatomical space, statistical models can be applied across the Jacobian determinant of the deformation fields, on a voxel-wise basis, to identify localized group volumetric differences (Lepore et al., 2008).

2.3.5. Voxel-based morphometry

In contrast to DBM, voxel-based morphometry (VBM) detects regional brain volume changes at the mesoscopic scale (i.e. several millimeters) (Ashburner et al., 1998). VBM is used to identify regional tissue volume differences in gray and white matter, and CSF (Ashburner & Friston, 2000). It is desirable to use DBM and VBM together because they complement each other by capturing brain volume changes at both the macroscopic and mesoscopic scales. Initially, MR scans are linearly transformed into a common anatomical space. This is followed by tissue classification, where each voxel will be assigned one of four classes: gray matter, white matter, CSF, or non-brain tissue. The resulting tissue maps are then blurred with a Gaussian kernel. Blurring is an important stage in VBM because it helps facilitate non-linear registration, performed later, by providing a better capture range for local displacements and mitigating registration errors. Blurring also permits Gaussian assumptions to be applied in later statistical analysis. If these tissue maps were not blurred, then complex discrete statistics would be required. The resulting blurred tissue maps are referred to as tissue density maps, which reflect the local concentration of each respective tissue (Ashburner & Friston, 2000). Finally, each tissue density map is non-linearly registered its corresponding tissue probability map, to account for global brain shape differences.

Statistical analysis can then be performed on a voxel-wise basis across the entire population to determine regional tissue volume differences. VBM can also incorporate a modulation step where the Jacobian determinant of the deformation field from the estimated non-linear transformation are multiplied with each voxel. By doing so, it will preserve the volume of particular tissues that may have been expanded or contracted during non-linear registration. When the modulation step is included the technique is referred to as optimized VBM (Good et al., 2001).

2.4. HIV-related MRI Studies

Since the discovery of HIV, structural MRI studies have used a variety of image processing methods to characterize and understand the extent of brain injury in HIV+ individuals. Studies published in the pre-HAART era reported significant volume loss in the basal ganglia, posterior cortex and total white matter in small number of HIV+ patients as compared to normal healthy controls (Aylward et al., 1995; Aylward et al., 1993; Heindel et al., 1994; Jernigan et al., 1993). Atrophy was reported to be more pronounced in advanced stages of cognitive impairment, but volume loss was still detected in cognitively normal HIV+ individuals (Stout et al., 1998).

In the HAART era, MRI studies continue to report significant brain volume loss in a wide variety of subcortical structures, such as the caudate (Ances et al., 2012; Becker et al., 2011; Cardenas et al., 2009; Kallianpur et al., 2013), thalamus (Cardenas et al., 2009; Chiang et al., 2007; Kallianpur et al., 2013), globus pallidus (Chiang et al., 2007), putamen (Becker et al., 2011; Chiang et al., 2007; Kallianpur et al., 2013), amygdala (Ances et al., 2012), hippocampus (Kallianpur et al., 2013) and corpus callosum (Ances et al., 2012; Chiang et al., 2007; Thompson et al., 2006). However, these patterns have not been universal: one study reported relatively increased putamen volume in an HIV+ cohort compared to age-matched controls (Castelo, Courtney, Melrose, & Stern, 2007).

Studies have also reported significant global volume changes, such as total gray matter (Becker et al., 2012; Cardenas et al., 2009; Cohen et al., 2010), white matter (Cardenas et al., 2009; Hua et al., 2013; Jernigan et al., 2011; Kallianpur et al., 2013), and cerebellar volumes (Cardenas et al., 2009; Kallianpur et al., 2013), as well as ventricular expansion (Cohen et al., 2010; Jernigan et al., 2011; Ragin et al., 2012; Thompson et al., 2006). Patients with AIDS-defining events were found to have a significant cortical thinning in the primary sensory and motor regions, and the occipital lobe (Thompson et al., 2005).

Volumetric changes in HIV+ patients have been shown to be significantly correlated with greater viral burden (viral load), immune response to the virus (nadir CD4+ cell count) and current immune system status (current CD4+ cell count). Several studies have reported that lower nadir CD4+ cell counts, indicating previous episodes of severe HIV-related immunosuppression, were significantly associated volume reductions in throughout the basal ganglia, total white matter, subcortical gray matter, frontal and temporal lobe, as well as greater CSF ventricular and sulcal enlargement (Cardenas et al., 2009; Cohen et al., 2010; Hua et al., 2013; Jernigan et al., 2011).

Lower current CD4+ cell counts were revealed to be significantly associated with corpus callosum, globus pallidus, putamen, and occipital lobe volume reductions, as well as ventricular enlargement (Chiang et al., 2007; Küper et al., 2011; Thompson et al., 2006). In contrast, higher current CD4+ counts, indicating stronger immune status, were unexpectedly correlated with lower white matter and subcortical gray matter volumes (Jernigan et al., 2011). This suggest that there may be a more complex relationship between brain integrity and current immune status.

Increasing viral loads have been shown to be associated with decreased caudate, thalamus, cerebellar and subcortical gray matter volumes (Cohen et al., 2010; Kallianpur et al., 2013). However, multiple studies have not detected any brain volume changes associated with viral loads (Chiang et al., 2007; Hua et al., 2013; Thompson et al., 2006; Thompson et al., 2005). The discrepancies between these studies could be dependent on treatment history of the study cohort. Despite good systemic viral suppression from HAART, viral reservoirs in the brain could contribute to on-going neuroinflammation. Thus, brain injury may still occur even though an HIV+ patient may have undetectable viral levels.

Although prior HIV-related MRI studies have provided key evidence into the impact HIV has on the brain, the reported patterns of atrophy across published studies are inconsistent. For example, many studies have reported that measures of immune status, and current and past infection severity (nadir CD4+ count, current CD4+ count and viral loads) are significantly associated with brain volume changes. However, other studies did not detect any associations with these measures and brain volumes (Ances et al., 2012; Aylward et al., 1993; Becker et al., 2011; Ragin et al., 2012). The lack of consistency across studies could be explained by several factors, including heterogeneity of both HIV+ and HIV- comparison groups, small sample sizes, variation in measurements of brain volumes, and the statistical methods applied to assess relationships with measures of immune status, and current and past infection severity. To produce a clear consensus

of the mechanisms that may underlie brain injury, and accurately characterize the pattern and extent of brain volume changes, the aforementioned factors must be addressed. Studies should report on large samples of treated HIV+ patients, with well-controlled infections, compared against a demographically similar HIV- control group, with advanced MRI processing techniques. The results from these studies will provide a good representation of the nature of brain injury in the HAART era.

2.5. Montreal Neurological Institute Image Processing Pipeline

The Montreal Neurological Institute (MNI) image processing pipeline is based upon the Medical Imaging NetCDF (MINC) file format and toolkit. It consists of many independent programs linked together to form a fully-automatic medical image processing pipeline. It will capture global and local brain volume measurements, and produce deformation fields and tissue density maps from each patient's MR scan. The flow chart in Figure 7 displays the major steps in the MNI image processing pipeline.

The pipeline begins with intensity non-uniformity correction. The signal captured from the human body within the MR scanner is rarely uniform, instead it varies smoothly across the image. This occurs because of poor RF coil uniformity, gradient-driven eddy currents and the fact that the patient is not entirely within the scanner's field of view (Sled, Zijdenbos, & Evans, 1998). It is important to remove the non-uniform intensity because some future processing steps, such as tissue classification, and linear and non-linear registration, heavily rely on intensity-based features. For example, two spatially separated voxels that contain the same tissue class may be classified as different tissues because they have different intensity values due to the non-uniformity.

Different methods have been developed to remove the intensity non-uniformity. For example, previous methods have combined tissue classification with non-uniformity correction (W. M. Wells, W. E. L. Grimson, R. Kikinis, & F. A. Jolesz, 1996b). In particular, Wells *et al.*, (Wells et al., 1996b), took advantage of the expectation-maximization (EM) algorithm to classify each voxel while simultaneously removing the non-uniformity. The EM method consists of two components, an expectation-step (E-step) and a maximization-step (M-step). The E-step will calculate the tissue class probabilities for each voxel given the current estimate of the non-uniformity field. Meanwhile, the M-step calculates the non-uniformity field given the current estimate of tissue class probabilities. The algorithm will alternate between the E- and M-step until a stopping criterion is met (Wells et al., 1996b).

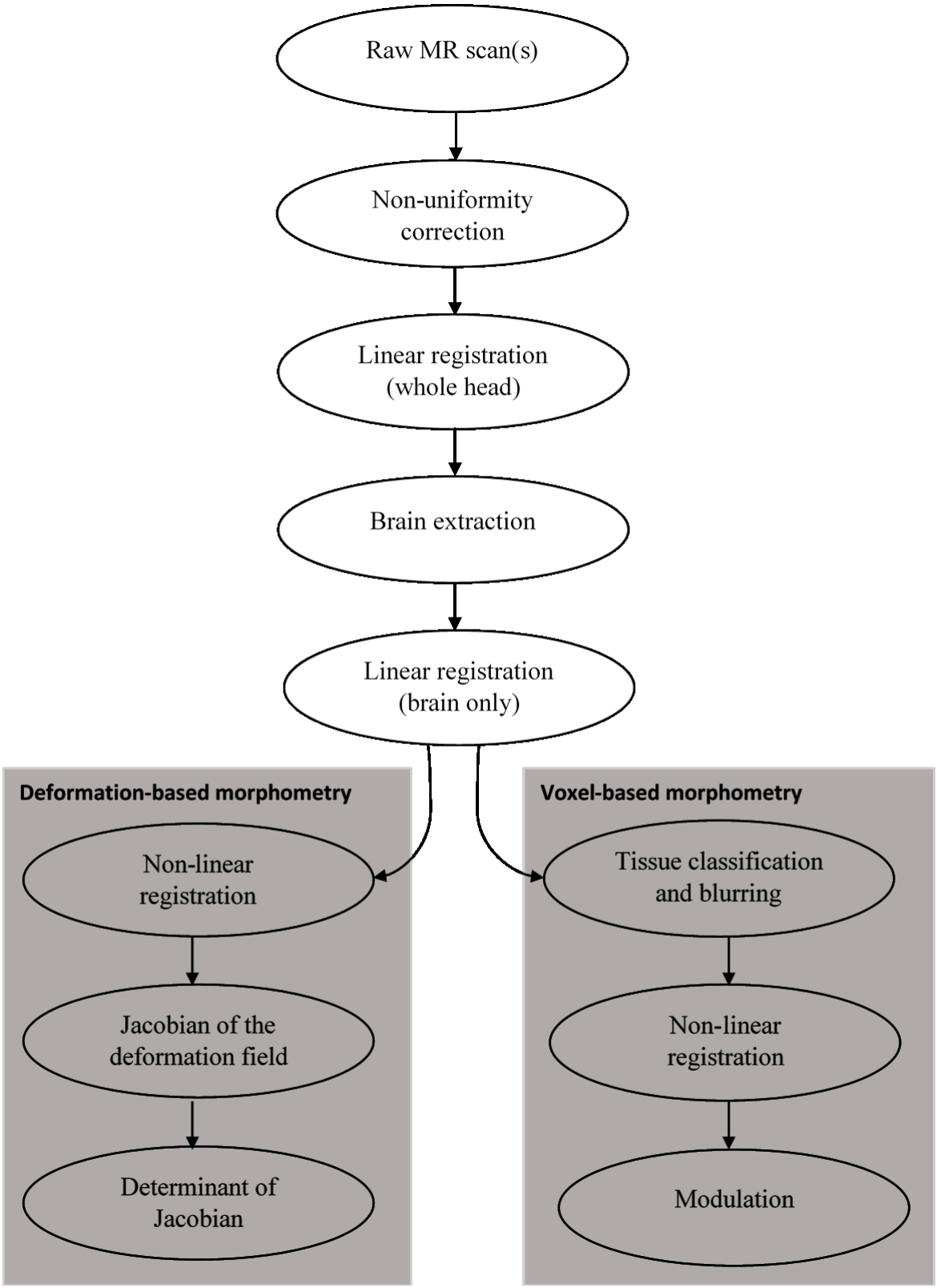

Figure 7: MNI image processing pipeline. Steps required to generate Jacobian determinant of the deformation fields and tissue density maps.

In our study, we utilized the nonparametric non-uniformity correction algorithm, known as N3 (Sled et al., 1998). To remove the non-uniformity, a smooth, slow varying field that maximizes the frequency content of the intensity distribution of the image is calculated (Sled et al., 1998). Once this smooth slow varying field is found, it is removed from the original image. In theory, the intensities across the MR scan should now be homogeneous. Figure 8 displays an example of an MR scan along with the intensity non-uniformity.

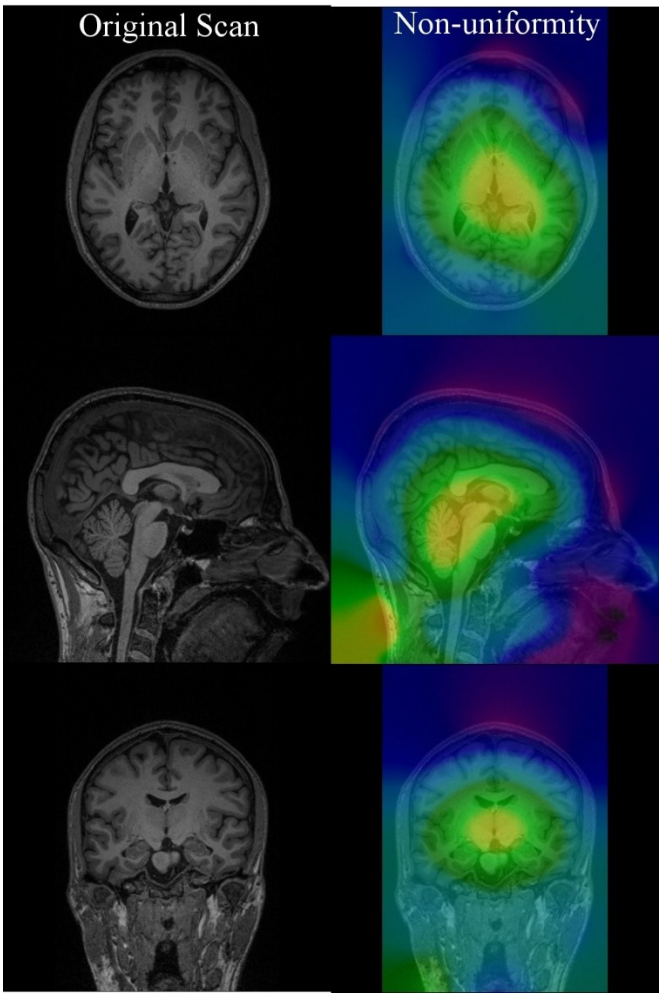

Figure 8: Example of an intensity non-uniformity across an MR scan. Notice in the brain regions beneath the skull, the image intensity is noticeably darker than the regions at the center of the brain. The intensity non-uniformity across the MR scan is caused by the inhomogeneous magnetic field in the MR scanner. It is important to remove such inhomogeneity before further image processing.

Recently, a variation of the N3 method, known as N4, was developed (Tustison & Gee, 2009). The N4 method improved the B-spline fitting, which allows for multiple resolutions to be used during the correction process. N4 also modifies the iterative update component such that the residual bias field is updated continuously (Tustison & Gee, 2009).

Following intensity non-uniformity correction, each MR head scan is transformed to the MNI stereotaxic space. The MNI stereotaxic space was based on the human brain atlas created by Talairach and Tournaux in 1988 (Talairach & Tournoux, 1988). It was known as the Talairach-Tournaux system and was used to map the location of brain structures into a common space independent of an individual's brain size and shape. However, this atlas did not account for the variability in brain size and shape across populations because it was based only on a single subject. To overcome this limitation, the International Consortium for Brain Mapping (ICBM) brain atlas was developed using the MRI data from 152 healthy adult subjects and is known as ICBM152. The procedure used to create the brain template included multiple iterations where, at each iteration, an individual's MR scan was non-linearly fitted to the average template from the previous iteration, beginning with the MNI152 linear template (Fonov, Evans, McKinstry, Almli, & Collins, 2009). This created an unbiased MRI template that can be used for medical image processing. In addition, the ICBM152 template included a tissue probability map and a fully-segmented structural atlas. These models play an important role for future processing steps such as tissue classification for VBM or brain structure segmentation for ROI analysis. The ICBM152 brain template is also used as a non-linear registration target, where patient's MR scans are warped to match the template. The ICBM152 brain template along with its associated label volumes are displayed in Figure 9.

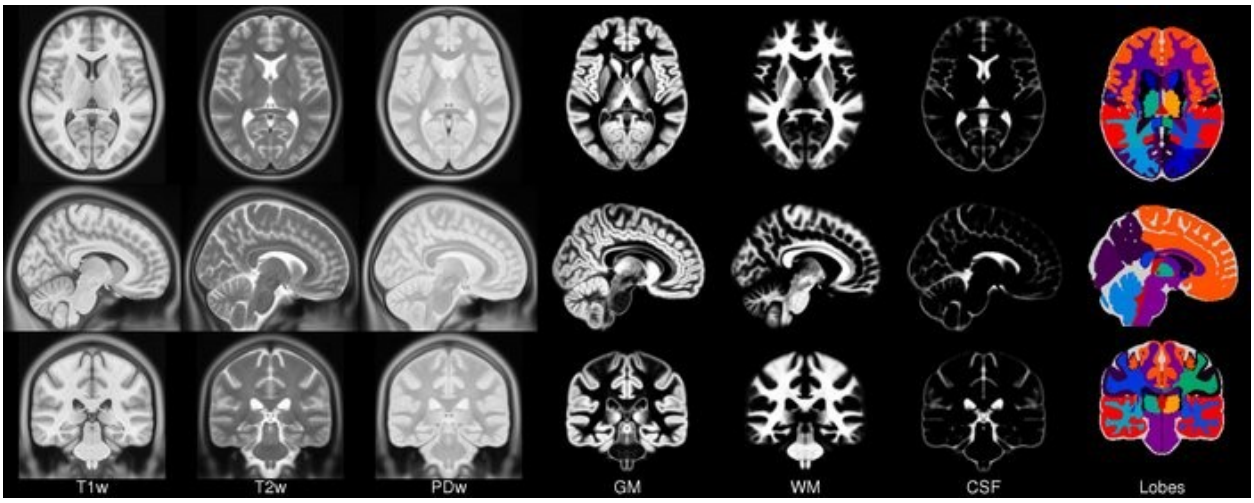

Figure 9: ICBM152 brain template, tissue probability maps and structural atlas (Fonov, 2009).

To transform each MR scan into the MNI stereotaxic space, they are linearly registered to the ICBM152 template via a nine-parameter affine transform, where the cross-correlation was used as the objective function (Collins, Neelin, Peters, & Evans, 1994). Cross-correlation is the measure

of similarity between two random variables. For image registration, the random variables are the source MR scan and the ICBM152 brain template. Maximizing the cross-correlation between the two images (on a voxel-by-voxel basis), theoretically, indicates that corresponding brain structures are aligned with each other. When the scans are transformed into the MNI stereotaxic space, it allows for future processing steps to take advantage of the tissue probability maps for tissue classification and the structural brain atlases for brain structure segmentation. In addition, since the scans are transformed to a common anatomical space, statistical models can be effectively applied on a voxel-by-voxel basis. However, due to non-linear morphological differences in normal anatomy between the individual's MR scan and the ICBM152 brain template, non-linear registration should be applied to improve the alignment of specific regions (Collins et al., 1995).

Following linear registration, the next step involves brain extraction or skull stripping using Brain Extraction based on nonlocal Segmentation Technique (BEaST) (Simon F. Eskildsen et al., 2012). Typically, MR head scans include the skull, dura and eyes, along with the brain (see Figure 4). Since future processing steps only focus on the brain, all tissues external to the brain are considered to be noise and should be removed. To do so, BEaST will create a brain mask that separates brain tissue from non-brain tissue. It classifies the following as brain tissues that should be included within the brain mask: cerebral and cerebellar gray and white matter, CSF in ventricles and the cerebellar cistern, CSF in deep sulci and along the surface of the brain and brainstem, and the brainstem itself (Simon F. Eskildsen et al., 2012). Meanwhile, non-brain tissues that should be removed include: skull, skin, muscles, fat, eyes, dura mater, bone, bone marrow, exterior blood vessels and exterior nerves, such as the optic chiasm (Simon F. Eskildsen et al., 2012). Figure 10 displays the brain mask created for one patient. Notice that the mask outlines the brain while excluding the skull, dura, eyes and other non-brain tissues. This mask will be used for all future processing steps.

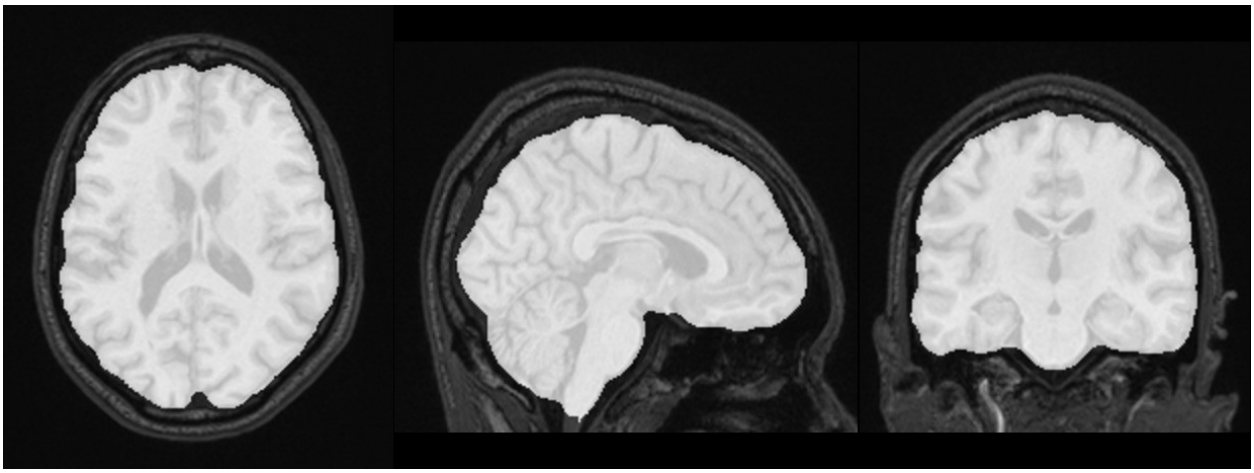

Figure 10: Brain mask created by BEaST.

After the brain mask for each patient has been created, the MR scans are linearly registered again to the MNI stereotaxic space. In contrast to the first linear registration, the second registration only aligns the masked brains, as opposed to the whole head, with the ICBM152 brain template. This increases the registration accuracy such that the corresponding brain structures are adequately aligned.

2.5.1. Deformation-based morphometry pipeline

Following the linear registration, ANIMAL (Automatic Nonlinear Image Matching and Anatomical Labeling) is used to non-linearly register MR scans to the ICBM152 brain template. It consists of a series of non-linear registration steps that are applied in a coarse-to-fine fashion, with each subsequent step refining the best previous registration transformation. ANIMAL requires sampling and stiffness parameters, which dictates the amount of deformation that should be applied to each participants MRI. The parameters can be chosen to minimize global shape differences, while retaining most of the local differences, or to maximize gross anatomical differences. For DBM, the sampling parameter was limited to a scale of 4 mm FWHM, with deformation vectors estimated every 2 mm. The stiffness parameter was kept low to enable each voxel to be optimally aligned with the corresponding voxel in the ICBM152 brain template.

The output from ANIMAL is a deformation field that maps each voxel of the subject's MRI to its corresponding location in the ICBM152 brain template volume (Collins et al., 1995). The Jacobian determinant was then applied to the deformation field to characterize local volume differences, at the voxel level, relative to the ICBM152 brain template (Chung et al., 2001). Figure 11 shows the initial source MR scan, resulting deformed source MR scan, target ICBM152 brain template and Jacobian determinant of the deformation field. As shown in Figure 11, the Jacobian

determinant of the deformation field shows the local brain growth and shrinkage at the voxel level. Since each individual's Jacobian is mapped into the MNI stereotaxic space, voxel-wise statistical analysis can reveal significant regions of brain growth or shrinkage and can be associated with infection status, and measures of current and past infection severity.

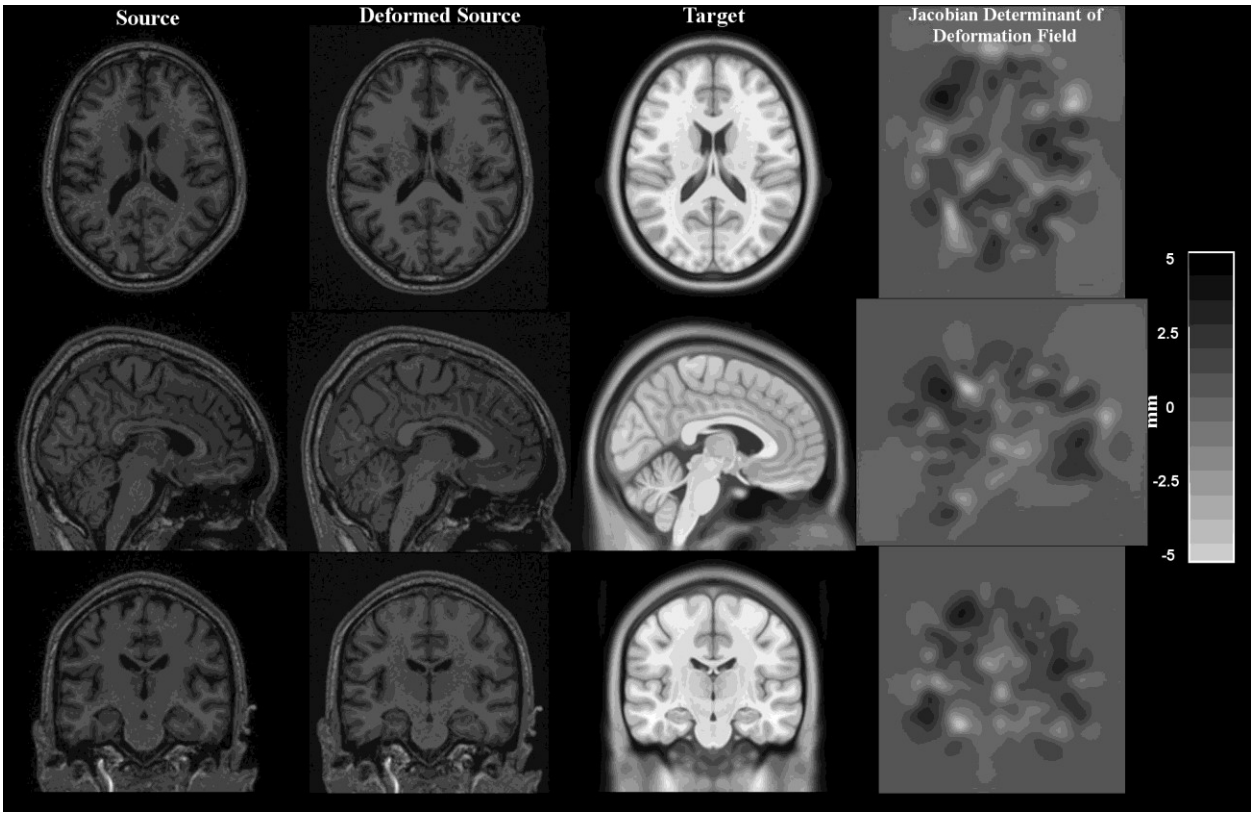

Figure 11: Column 1: Source MR scan. Column 2: Deformed source. Column 3: Target ICBM152 brain template. Column 4: Jacobian determinant of the deformation field revealing regions of local brain growth and shrinkage.

2.5.2. Voxel-based morphometry pipeline

At this point in the VBM pipeline, the raw MR scans have been corrected for intensity non-uniformity, skull stripped and linearly transformed into the MNI stereotaxic space. The next step is tissue classification, where each voxel is assigned one of four classes: gray matter, white matter, CSF, or non-brain tissue. This process will take advantage of the tissue probability map provided by the ICBM152 brain atlas to train an artificial neural network classifier based on the voxel intensity characteristics (Zijdenbos et al., 2002). Figure 12 displays the results of tissue classification for one patient. Following tissue classification, each tissue map was smoothed with an isotropic Gaussian kernel of 8 mm FWHM, resulting in the tissue density maps. A FWHM of 8 mm was chosen because it increases the signal-to-noise ratio to capture volumetric changes, but does not severely distort important features. ANIMAL was used to non-linearly register each tissue

density map with its corresponding tissue probability map. This accounts for global brain shape differences among individuals (Collins et al., 1995; Good et al., 2001). The sampling and stiffness parameters were chosen to minimize global brain shape differences, and capture most of the local volume differences. However, as a result of non-linear registration, the volumes of certain brain regions may grow, whereas others may shrink. To preserve tissue volumes, the Jacobian determinant of the non-linear transform was multiplied to each voxel of the tissue density maps (Good et al., 2001). Voxel-wise statistical analysis can be performed on each tissue density map, revealing regions of significant brain volume and tissue concentration changes across study populations.

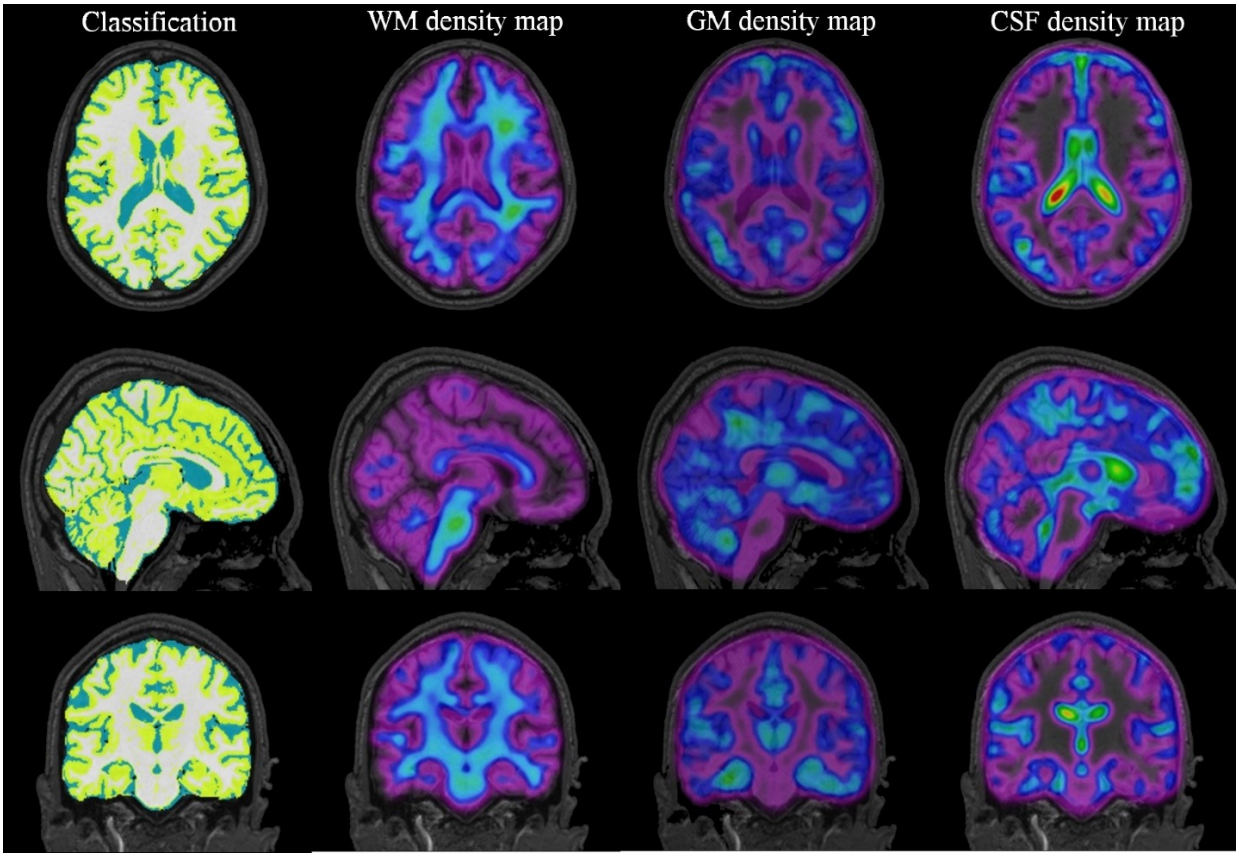

Figure 12: Column 1: Colour-coded classification of the three tissue types in the brain. Column 2-4: Modulated tissue density maps of each respective tissue type. Tissue density maps reveal local concentration of respective tissue.

2.6. Statistical Analysis

Once the Jacobian determinant of the deformation fields and tissue density maps are produced for each patient, statistical analysis can be used to identify significant regional brain volume changes. The analysis is performed on a voxel-by-voxel basis since all the resulting maps

are in a common anatomical space. This means that each voxel across all scans, theoretically, correspond to the same brain region and tissue.

The most commonly used statistical model for VBM and DBM analysis is the general linear model (GLM). It tests the effects of a series of explanatory variables, such as HIV status, nadir CD4+ cell counts, current CD4+ cell counts, or viral load, and demographic factors, against a dependent variable, which, in our case, will be the Jacobian determinant of the deformation fields or the intensity of the tissue density maps. This model assumes the relationship between the dependent and independent variables are linear. For our analysis, we separately test for the effects of HIV status, nadir CD4+ cell counts, current CD4+ cell counts and viral load, while controlling for the effects of age, gender, education and ethnicity. Equation 3 shows the typical linear model that we will use, where *Maps* is the either the Jacobian determinant of the deformation fields or one of the three modulated tissue density maps.

$$Maps = \beta_0 + \beta_1 \cdot Age + \beta_2 \cdot Gender + \beta_3 \cdot Education + \beta_4 \cdot Ethinicity + \beta_5 \cdot Covariate\ of\ interest$$

Equation 3: General Linear Model.

The GLM regressions that are computed at each voxel must be evaluated for statistical significance, i.e., the *p*-value of each regression must be evaluated. The *p*-values at each voxel create statistical maps that help visualize the brain and tissue volume changes associated with some covariate. However, since these statistical tests are conducted on voxel-by-voxel basis, upwards of 750,000 tests are performed across the entire brain simultaneously. Based on simple probability, a typical confidence region of 5% (i.e., $p < 0.05$) will result in approximately 37,500 voxels that will be considered statistically significant in a volume containing only random noise. This means that DBM and VBM analysis are highly susceptible to false positives. It is important account for false positives via multiple comparisons correction.

Several methods have been developed to control the number of false positives, such as Bonferonni's correction, Gaussian Random Field Theory and False Discovery Rate (FDR). Bonferonni's correction is one of the most standard and simplest ways to account for multiple comparisons. To compute it, the desired significance is divided by the number of comparisons performed. For example, if a significance of $p < 0.05$ is desired and the number of comparisons is 750,000, then a voxel must be $p < 0.000000067$ to be statistically significant. Clearly, Bonferonni's correction is very stringent, and susceptible to removing true positives along with false positives.

Gaussian Random Field Theory is an extension of Bonferonni's correction developed by Worsley *et al.* (Worsley, Andermann, Koulis, MacDonald, & Evans, 1999). It assumes that not all tests are independent, but the actual number of independent units are much smaller due to imperfect registration and blurring (Worsley et al., 1999). Although this method has been utilized by several studies, it is also known to be a stringent thresholding technique (Genovese, Lazar, & Nichols, 2002).

In our case, we used the False Discovery Rate (FDR) to control the number of false positives. FDR takes a different approach to thresholding. In contrast to previous thresholding techniques that used a strong correction for multiple comparisons, FDR is more lenient. For example, random field theory states that 19 times out of 20 there will be no false positives in the resulting threshold, when the significance is $p < 0.05$. Meanwhile, FDR states that of all the results shown in the image, 5% on average will be false positives (Genovese et al., 2002). By using FDR, there is increased sensitivity while losing the same level of certainty as provided with random field theory (Genovese et al., 2002).

Chapter 3: Regionally Specific Brain Volume Reductions in HIV+ Patients in the HAART era

Authors: Ryan Sanford[1], Ana Lucia Fernandez Cruz[1], Lesley K. Fellows[1], Beau. M. Ances[2] and D. Louis Collins[1*]

[1] Montreal Neurological Institute, McGill University, 3801 University Street, Montréal, Québec, Canada H3A 2B4

[2] Department of Neurology, Washington University, Box 8111, 660 South Euclid, St. Louis, Missouri, USA 63110

*Corresponding author: D. Louis Collins, PhD

Address:
McConnell Brain Imaging Center WB-314
Montreal Neurological Institute
3801 University St.
Montreal, Quebec
CANADA H3A 2B4

Phone:
1-514-398-4227

Email:
louis.collins@mcgill.ca

3.1. Preface

Chapter 2 provided a detailed overview of HIV and the potential mechanisms that cause brain injury. This was followed by an in-depth review of magnetic resonance imaging and medical image processing techniques. The following chapter takes the form of a manuscript, where the effects HIV has on the brain were investigated. Although several studies have examined brain volume changes in HIV+ individuals, the reported patterns of brain injury were very inconsistent. Discrepancies between the studies reflect differences in the degree of infection and impairment severity in the HIV+ cohort, small sample sizes, and the MRI processing methods utilized vary in statistical power and technical limitations. In the proceeding study, we report on a large sample of HIV+ patients with deformation- and voxel-based morphometry. The results from our study provide a detailed illustration of the effect HIV has on the brain in treated HIV+ patients with well-controlled infections. This manuscript will be submitted to the *AIDS* journal because it allows our findings to be viewed by all the top clinicians and researchers in the HIV/AIDS community.

3.2. Abstract

The HIV infection is commonly associated with cognitive impairment even when systemic viral replication is effectively suppressed with highly active anti-retroviral therapy (HAART). The underlying pathophysiology of this impairment remains unclear. In an effort to understand the pattern and extent of brain volume changes caused by the infection, we utilized deformation-based morphometry and voxel-based morphometry to investigate the correlation of regional brain volumes in HIV+ patients against demographically similar normal healthy controls, and measures of immune status, and current and past infection severity. We observed significant volume loss in the brainstem and thalamus of our HIV+ cohort compared to normal healthy controls. In addition, patients with a history of more severe immunosuppression had significant atrophy in the brainstem, thalamus, caudate, globus pallidus, internal capsule and right frontal lobe, as well as greater enlargement of the third ventricle. These results suggests that early initiation of HAART may be important in protecting long term brain health, and shows that some brain regions are more vulnerable to the effects of HIV-related immunosuppression.

3.3. Introduction

HIV enters the brain soon after seroconversion and can cause cognitive impairment (Masters & Ances, 2014). Although the advent of highly active anti-retroviral therapy (HAART) has reduced the incidence of severe dementia (Antinori et al., 2007; Schouten, Cinque, Gisslen, Reiss, & Portegies, 2011), the prevalence of mild to moderate cognitive impairment appears to be increasing (Ances & Ellis, 2007; Heaton et al., 2011a). It has been reported that 30-50% of patients, currently treated with HAART, show minor cognitive deficits (Simioni et al., 2010). Several factors are suspected to contribute to this milder impairment, including indirect effects of comorbidities, aging and treatment side effects. In principle, brain injury directly related to HIV could have occurred at the time of untreated HIV infection, prior to diagnosis or prior to HAART initiation, or could be related to on-going HIV infection. It has been proposed that limited anti-retroviral therapy penetrance of the blood-brain barrier may lead to a reservoir of HIV replication within the central nervous system (CNS), despite good systemic viral control (Ellis, Langford, & Masliah, 2007).

Structural magnetic resonance imaging (MRI) has provided key evidence concerning the topography of brain changes due to HIV. Studies published in the pre-HAART era reported significantly smaller volumes within specific brain structures including the basal ganglia, posterior cortex, and total white matter in a small number of HIV+ patients compared to healthy controls (Aylward et al., 1995; Aylward et al., 1993; Heindel et al., 1994; Jernigan et al., 1993). More pronounced volumetric loss was observed in HIV+ patients with greater cognitive impairment, but smaller brain volumes were detected even in cognitively normal HIV+ individuals (Stout et al., 1998).

Although MRI studies continue to report significant brain volume loss in a wide variety of subcortical and cortical regions in the HAART era (Holt et al., 2012; Masters & Ances, 2014), the reported patterns of atrophy across published studies are inconsistent. For example, some studies have reported that smaller brain volumes were significantly associated with viral load, nadir CD4+ counts, or current CD4+ counts (Cardenas et al., 2009; Chiang et al., 2007; Cohen et al., 2010; Hua et al., 2013; Jernigan et al., 2011; Kallianpur et al., 2013; Küper et al., 2011; Thompson et al., 2006; Thompson et al., 2005). Meanwhile, other studies did not observe any associations with measures of immune status, or current and past infection severity (Ances et al., 2012; Aylward et al., 1993; Becker et al., 2011; Ragin et al., 2012). The lack of consistency across studies could be

explained by several factors, including heterogeneity of both HIV+ and HIV- comparison groups, small sample sizes, variation in measurements of brain volumes, and the statistical methods applied to assess relationships with measures of immune status, current and past infection severity.

The majority of existing structural MRI studies have used region of interest (ROI)-based volumetric analysis (Ances et al., 2012; Aylward et al., 1995; Aylward et al., 1993; Becker et al., 2011; Castelo et al., 2007; Cohen et al., 2010; Heindel et al., 1994; Jernigan et al., 1993; Jernigan et al., 2011; Kallianpur et al., 2013; Ragin et al., 2012; Stout et al., 1998; Thompson et al., 2006). Although ROI-based methods have been widely used to detect brain volume changes in a range of disorders, these methods typically require prior hypotheses about where volumetric differences will be found, particularly when applied in small samples (Chung et al., 2001). These hypothesis-driven experiments cannot discover unpredicted volume differences, and when statistical power is low, null findings may not provide additional information. The results of ROI-based studies are also sensitive to the brain structure segmentation method used, speaking to the considerable analytic challenges in the rapidly evolving neuroimaging field (Dewey et al., 2010). Alternative approaches have been developed to detect structural abnormalities that do not depend on *a priori* anatomical hypotheses (Ashburner & Friston, 2000). These include deformation-based morphometry (DBM) and voxel-based morphometry (VBM). These techniques search the whole brain simultaneously at voxel level (i.e. 1 x 1 x 1 mm^3) for between-group differences, and can also test for correlations with explanatory variables at the same high spatial resolution.

One widely-used form of DBM estimates a brain volume difference, on a voxel-by-voxel basis, relative to an average brain template (Ashburner & Friston, 2000; Chung et al., 2001). VBM, in contrast, involves a voxel-wise comparison of the local concentrations of gray matter, white matter, and cerebrospinal fluid (CSF) space between populations (Ashburner & Friston, 2000). While both methods have been successfully applied to several neurodegenerative disorders (e.g. Alzheimer's Disease (Baron et al., 2001; Hua et al., 2008) and Parkinson Disease (Beyer, Janvin, Larsen, & Aarsland, 2007; Borghammer et al., 2010)), they have not often been used to study the effects HIV has on the brain in the HAART era.

The aims of the study were to characterize the nature and extent of regional brain volume differences between HIV+ individuals and a demographically similar HIV- group, and to assess whether measures of immune status, and current and past HIV infection severity are related to measures of regional brain volume. We applied advanced neuroimaging analytic methods: DBM

and VBM, to structural MRIs acquired in a large sample of HIV+ patients drawn from a US infectious disease clinic, and a healthy HIV- comparison group drawn from the local community. We report regionally-specific patterns of reduced subcortical volumes in the HIV+ sample, despite HAART yielding full viral suppression in the majority. Reduced white matter and subcortical volumes were related to nadir CD4 counts. However, current viral suppression and immune status did not relate to any regional brain volume changes. Overall, the results provide a detailed picture of the impact HIV has on regional brain volumes in a large sample of HAART-treated HIV+ patients, and suggests that distinct mechanisms may underlie subcortical injury.

3.4. Materials and Methods

3.4.1. Subjects

One hundred thirty-three HIV+ participants were recruited from the Infectious Disease clinic at Washington University in St. Louis, while fifty-eight healthy controls were recruited from the local community. Each participant provided written consent approved by the Institutional Review Board at Washington University. Individuals with a history of confounding neurological disorders including epilepsy, stroke, and head injury resulting in a loss of consciousness greater than 30 minutes, major psychiatric disorders, or active substance abuse were excluded. Serological status of all HIV+ participants was confirmed by documented positive HIV enzyme-linked immunoassay and Western blot or detection of plasma HIV RNA by polymerase chain reactions. Table 1 summarizes the cohort demographics, and clinical characteristics. The majority of the HIV+ patients had effective viral suppression, and 90% of the patients were currently receiving stable HAART.

	HIV+ (n=133)	HIV- (n=58)	p value
Demographics			
Mean age (years old)	47.8 ± 12.2	42.6 ± 12.3	**0.01**
Sex (% Male)	64	55	0.27
Education (years)	14.4 ± 2.8	15.2 ± 2.1	**0.02**
Ethnicity			0.25
% African American	69	58	
% Caucasian	29	42	
% Other	2	0	
Clinical and Neuropsychological Characteristics			
Duration of HIV infection (months)	135 ± 99	NA	NA
% receiving HAART	90	NA	NA
Central Nervous System Penetration Effectiveness (CPE) Score	6.73 ± 3.06	NA	NA
Laboratory			
Median CD4 (cells/μL) (Quartiles)	520 (267, 711)	NA	NA
Median nadir CD4 (cells/μL) (Quartiles)	189 (40, 319)	NA	NA
Median Log Plasma Viral Load (copies/mL) (Quartiles)	1.31 (1.30, 1.94)	NA	NA
% Virologically Suppressed (<50 copies/mL)	72	NA	NA

Table 1: Demographic and clinical characteristics of participants.

3.4.2. Structural MRI acquisition

All participants underwent contemporaneous MR scanning using a 3T Siemens Tim TRIO whole-body magnetic resonance scanner (Siemens AG, Erlangen, Germany) with a transmit/receive head coil. Structural imaging was acquired using a T1-weighted three dimensional magnetization-prepared rapid acquisition gradient echo (MPRAGE) sequence (TR = 2400 ms, TE = 3.16 ms, flip angle = 8˚, and voxel size = 1 mm^3). Images were visually inspected at the scanner with an additional scan performed if significant movement was observed.

3.4.3. Image Processing

Initially, each individual's MRI underwent automated correction for intensity non-uniformity due to radiofrequency inhomogeneity using N3 (Sled et al., 1998). All scans were spatially normalized to the ICBM152 average brain template by linear registration using a nine-parameter affine transform (Collins et al., 1994). After these pre-processing steps, the MRI data was ready for DBM and VBM, as described below.

3.4.4. Deformation-based morphometry

DBM analysis estimates a surrogate of brain volume difference, on a voxel-by-voxel basis, compared to the ICBM152 average brain template. A series of non-linear registration steps were applied in a coarse-to-fine fashion, with each subsequent step refining the best previous registration transformation, resulting in a deformation field that maps each voxel of the subject's MRI to its corresponding location in the ICBM152 brain template volume (Collins et al., 1995). A Jacobian matrix field was computed from the resulting deformation field with the determinant of the Jacobian matrix used to characterize local volume differences, at the voxel level, relative to the ICBM152 brain template (Ashburner & Friston, 2000; Ashburner et al., 1998; Chung et al., 2001). Voxel-wise statistical analysis was performed to identify regions of statistically significant brain growth and shrinkage.

3.4.5. Voxel-based morphometry

In contrast to DBM, VBM is used to identify regional brain tissue volume differences in gray and white matter, and CSF space (Ashburner & Friston, 2000; Good et al., 2001). After the scans were spatially normalized, an artificial neural network classifier algorithm was used to assign each voxel into one of four classes: gray and white matter, CSF, and non-brain tissue (Zijdenbos et al., 2002). Following tissue classification, each tissue map was smoothed with an isotropic Gaussian kernel of 8 mm FWHM, resulting in tissue density maps. These maps reflect the local concentration of each respective tissue (Ashburner & Friston, 2000). The tissue density maps were then non-linearly registered to the ICBM152 brain template to account for global brain shape differences (Collins et al., 1995). Then the Jacobian determinant from the non-linear transform was applied to each voxel to preserve tissue volumes (Good et al., 2001). Voxel-wise statistical analysis was performed on each tissue density map across populations to reveal regions of significant tissue volume changes (Ashburner & Friston, 2000).

3.4.6. Statistical Analysis

Linear regression analyses was used to compare the Jacobian determinant of the deformation fields and tissue density maps in HIV+ and HIV- groups, and correlate them against measures of immune status, and current and past infection severity (e.g. nadir CD4+ cell count, current CD4+ cell count and viral load) in the HIV+ group. Each of the regression models included age, gender, ethnicity and education as covariates. In addition, the viral loads were log-transformed

and the CD4+ count variables were square root transformed to normalize the distributions and stabilize the variances. Statistical maps were generated to illustrate patterns of significant brain and tissue volume changes. All statistical maps were corrected for multiple comparisons using the standard false discovery rate (FDR) method, with a false-positive rate of 5% or q=0.05 (Genovese et al., 2002).

3.5. Results

3.5.1. Voxel-based morphometry

The VBM results indicate that HIV+ individuals had significantly smaller white matter volume in the brainstem and thalamus compared to healthy controls (Figure 13). In contrast, no significant gray matter or CSF volume differences were detected in HIV+ patients, after controlling for demographic factors and correcting for multiple comparisons.

Among HIV+ individuals, a strong relationship was observed between lower nadir CD4+ counts and smaller white matter volumes in the brainstem, globus pallidus, internal capsule, right frontal lobe, and caudate (Figure 14). Lower nadir CD4+ counts were also significantly associated with greater CSF volume (presumably reflecting dilatation ex-vacuo) in the third ventricle and cerebellar cistern.

In contrast, current CD4+ counts and viral load were not significantly correlated with any volume changes within the HIV+ cohort. In addition, no significant volume differences were revealed between HIV+ patients with currently detectable and undetectable viral loads.

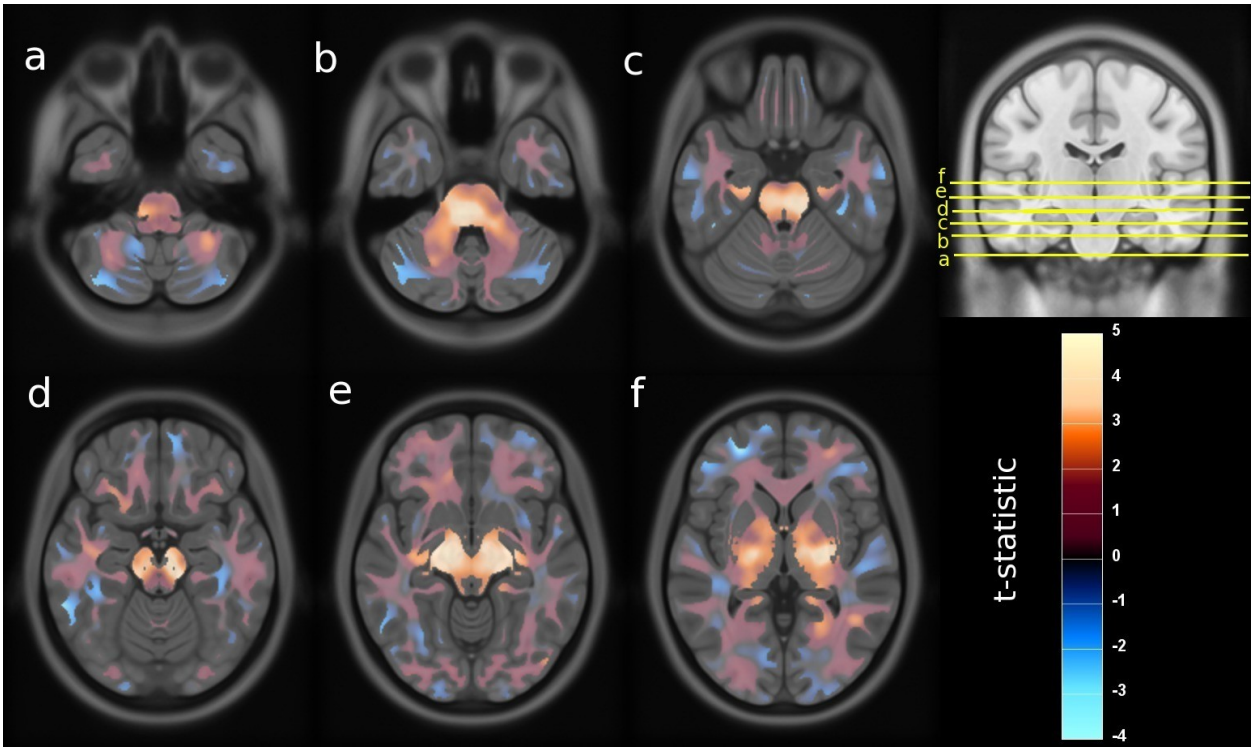

Figure 13: White matter volume differences in HIV- comparison group relative to the HIV+ patients. Blue colours denote a negative correlation and red colours denote a positive correlation, where positive correlations correspond to smaller tissue volumes. Regions with absolute *t*-values greater than 3.10 were considered statistically significant (at the FDR level of 0.05).

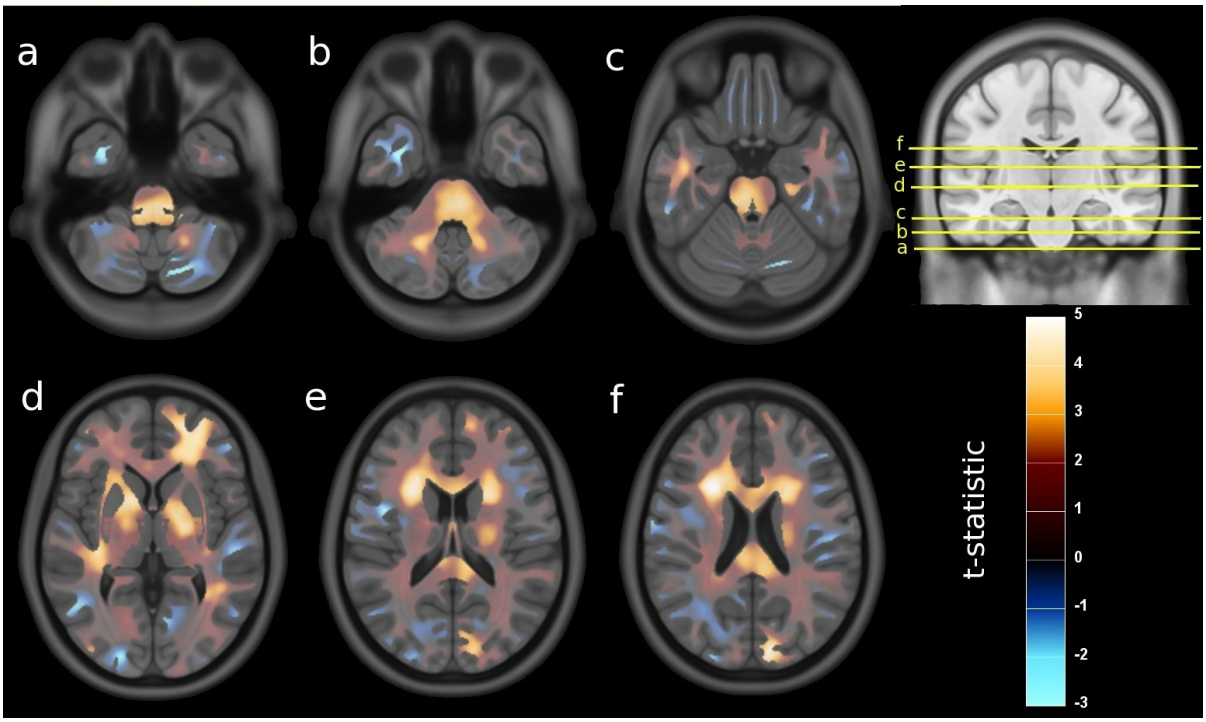

Figure 14: Lower white matter volumes associated with lower nadir CD4+ counts. Orange colors indicate lower white matter volumes associated with lower nadir CD4+ counts. Regions with absolute t-values greater than 3.42 were considered statistically significant (at the FDR level of 0.05).

3.5.2. Deformation-based morphometry

Unlike the results from VBM, DBM analysis did not reveal any significant volume changes in HIV+ patients compared to healthy controls. However, lower nadir CD4+ counts were significantly associated with smaller volumes of the brainstem, thalamus, caudate, globus pallidus and frontal lobe, as well as enlargement of the third ventricle (Figure 15). No significant volume changes associated current CD4+ counts or viral load were detected. In addition, there were no significant differences between HIV+ patients with detectable and undetectable viral loads, after controlling for demographic factors and correcting for multiple comparisons.

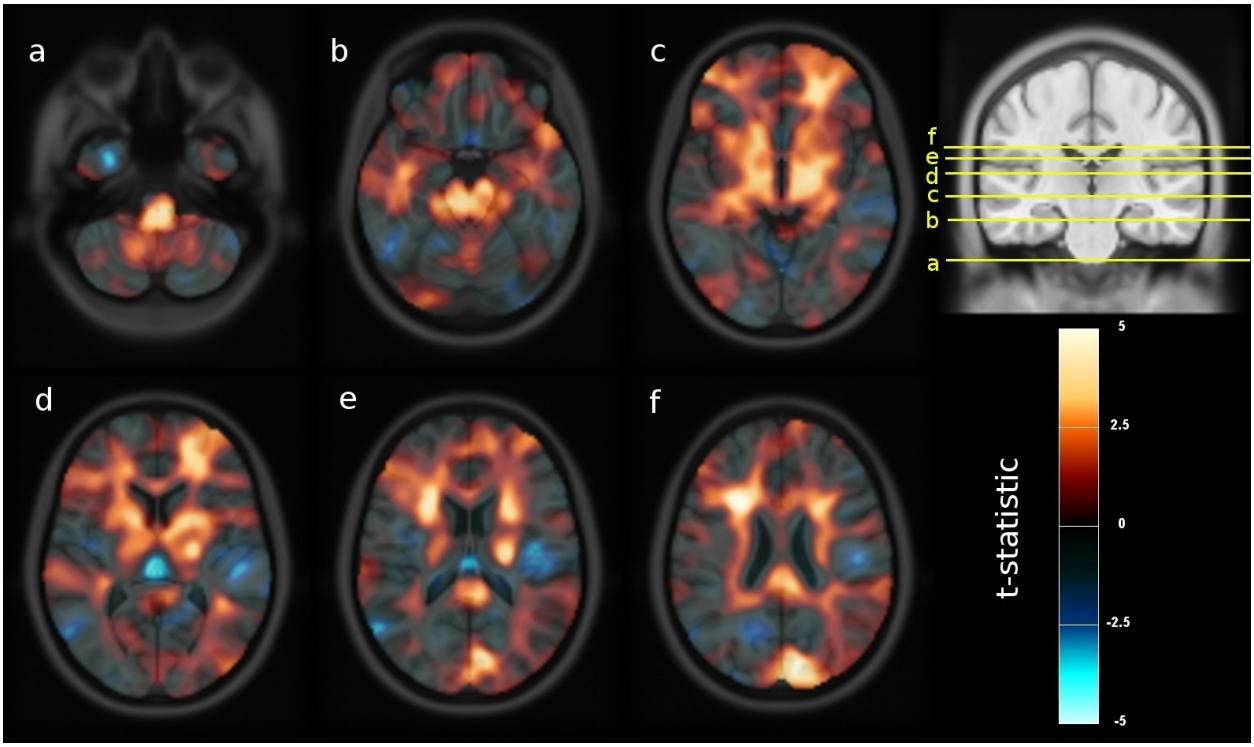

Figure 15: Smaller brain volumes associated with lower nadir CD4+ counts overlaid in the ICBM152 template. Orange colors indicate reduced brain volumes associated with lower Nadir CD4+ counts. Regions with absolute t-values greater than 3.30 were considered statistically significant (at the FDR level of 0.05).

3.6. Discussion

Existing HIV-related MRI studies have provided considerable evidence of the pattern and extent of brain volume changes in HIV+ patients (Holt et al., 2012; Masters & Ances, 2014). However, this literature has yet to produce a clear consensus of the mechanisms that may underlie brain injury. Inconsistency across studies reflect several factors, including differences in the degree of infection and impairment severity in the HIV+ cohort, small sample sizes, and the MRI processing methods utilized vary in statistical power and technical limitations. Here, we report on

a large sample of HIV+ patients drawn from a US infectious disease clinic and a demographically similar HIV- community-based comparison group. Nearly all of the HIV+ subjects were on stable HAART treatment, and the majority had full viral suppression. We applied advanced MRI processing techniques with complementary strengths in assessing brain structures volumes: DBM and VBM, to provide evidence of the regionally-specific effects the infection has on the brain. We compared brain measures in the HIV+ and HIV- groups, and related the measures with indices reflecting current and past infection severity.

After controlling for demographic factors, we found evidence of widespread group differences in subcortical and brainstem structures. VBM revealed smaller white matter volumes that were particularly marked in the brainstem, cerebellar peduncles and thalamus, as well as in the periventricular white matter of the cerebral hemispheres. This method, however, did not identify any group differences in gray matter or CSF volumes. DBM, which captures the brain growth and shrinkage relative to the ICBM152 brain template, revealed no significant group differences. However, regional patterns of brain volume loss similar to those seen with VBM were evident at more lenient statistical thresholds.

Multiple studies have reported significant volume reductions in subcortical structures that were also most pronounced in the brainstem and thalamus. Using tensor-based morphometry, a technique similar to DBM, Chiang *et al.,* (Chiang et al., 2007), observed significant subcortical volume loss, including the thalamus, in a sample of 26 AIDS patients. Küper *et al.*, (Küper et al., 2011), utilized VBM to reveal significant white matter volume loss in the midbrain of HIV+ patients with cognitive decline. Using ROI analysis, Kallianpur *et al.,* (Kallianpur et al., 2013), reported reduced thalamic and brainstem volumes in a small sample HIV+ patients compared to healthy controls. Pfefferbaum *et al.*, (Pfefferbaum et al., 2012), detected smaller thalamic volumes in 59 HIV+ patients, using ROI analysis, compared to 108 healthy controls. Finally, Janssen *et al.,* (Janssen et al., 2015), also used ROI techniques to observe reduced thalamic volumes in a study population similar to the one we have reported on. Although the aforementioned studies differ in sample size, cohort characteristics, and MRI processing techniques, our finding of reduced thalamic and brainstem volume appears to be consistent with the literature.

In contrast, we did not see significant group differences, using either VBM or DBM, in other basal ganglia structures, despite the sensitivity afforded by the relatively large sample size. In a previous study, Ances *et al.*, (Ances et al., 2012), used ROI analysis to reveal volume loss in

the corpus callosum, caudate and amygdala in 52 HIV+ patients, 50% of whom were untreated. Utilizing a fully deformable segmentation routine, Becker *et al.*, (Becker et al., 2011), found caudate and putamen atrophy, principally in the anterior regions, of 84 HIV+ patients. In a cohort of AIDS patients, several of whom were untreated, Thompson *et al.*, (Thompson et al., 2006), and Chiang *et al.*, (Chiang et al., 2007), reported volume loss in the globus pallidus, putamen, internal capsule, corpus callosum, as well as ventricular enlargement. Kallianpur *et al.*, (Kallianpur et al., 2013), revealed significant volumetric reductions in the hippocampus, caudate, putamen, and nucleus accumbens in an HIV+ cohort with ineffective viral suppression in the majority. We may not have detected volume loss in these basal ganglia structures because the majority of our HIV+ patients were treated and had effective viral suppression, unlike the previous studies. Together, these results suggest that widespread subcortical atrophy most likely occurs in untreated HIV+ subjects with uncontrolled and late-stage HIV infections.

However, the consistent effects in the thalamus and brainstem, and the apparent selectivity of effects to the white matter compartment in these regions, may provide clues to the underlying pathophysiology. In particular, it could suggest on-going brain injury, perhaps related to CNS viral reservoirs. It has been shown that reservoirs of multinucleated giant cells and microglial nodules form in central white matter and basal ganglia regions, accompanied by infiltration of virus-induced microglia, macrophages and astrocytes, leading to axonal damage, neuronal apoptosis and ultimately brain atrophy (Bell, 2004; Lawrence & Major, 2002). This neuropathology could also explain the apparent proclivity for particular subcortical structures reported throughout the literature. In addition, since HIV enters the brain soon after seroconversion, long-lived infected microglia in the CNS could contribute to neuronal apoptosis (Gray et al., 1996; Lambotte, Deiva, & Tardieu, 2003; Masters & Ances, 2014). This suggest that initiating HAART soon after seroconversion may be important in protecting long term brain health, since it would prevent significant amounts of HIV from entering the CNS.

To assess whether brain volume changes were related to direct effects of the infection, brain volume measures were correlated against indices of infection severity in the HIV+ group. Both DBM and VBM analysis revealed that patients with a history of more severe HIV-related immunosuppression, as indicated by lower nadir CD4+ counts, had significantly smaller white matter volumes in the brainstem, thalamus, caudate, globus pallidus, internal capsule and right frontal lobe, as well as greater enlargement (presumably ex-vacuo) of the third ventricle. These

results agree with previous studies that reported significantly smaller volumes throughout the basal ganglia and frontal lobes, as well as larger ventricles, associated with lower nadir CD4+ counts in HIV+ patients (Cardenas et al., 2009; Cohen et al., 2010; Hua et al., 2013; Jernigan et al., 2011). This suggests that widespread subcortical volume loss is linked to events triggered at the time of untreated HIV infection, which implies that early treatment with HAART may avoid long term brain injury.

Consistent with many studies, we did not detect significant relationships between indices of current HIV infection (current CD4 count and viral suppression) and regional brain volume changes (Ances et al., 2012; Aylward et al., 1993; Becker et al., 2012; Becker et al., 2011; Hua et al., 2013; Ragin et al., 2012). However, multiple reports in the literature reported significant associations between these measures and brain volumes. Lower current CD4+ counts were significantly associated with middle cingulate, corpus callosum, globus pallidus and putamen volume reductions, as well as ventricular expansion in a small cohort of AIDS patients, 50% of whom were untreated (Chiang et al., 2007; Thompson et al., 2006). Meanwhile, higher current CD4+ counts were unexpectedly correlated with lower white matter and subcortical gray matter volumes, as well as increased CSF, in a large cohort of HIV/AIDS patients (Jernigan et al., 2011). HIV+ individuals with detectable viral loads had decreased cerebellar, subcortical gray matter, and cortical white matter volumes, as compared to individuals with undetectable viral loads and normal healthy controls (Cardenas et al., 2009; Kallianpur et al., 2013). In a study where 14% of the HIV+ patients had advanced AIDS dementia, viral loads were reported to be significantly associated with lower caudate and thalamus volumes, as well as ventricular expansion (Cohen et al., 2010). These findings suggest that there may be a more complex, perhaps non-linear, relationship between the brain integrity and measures of current HIV infection severity. In addition, discrepancies between the findings could, in part, be explained by the infection severity of the study cohorts. The majority of the aforementioned studies consisted of untreated HIV+ patients with AIDS-defining events or ineffective viral suppression, whereas we report on an HIV+ group on stable treatment and well-controlled infection in the majority.

Although this study has provided a detailed illustration of the impact HIV has on regional brain volumes, it is difficult to make causal inferences since these findings are based on cross-sectional analysis. To validate these results, additional longitudinal studies are required. Our study also could not determine the protective effects of the HAART CNS penetration effectiveness on

brain volume changes. To determine such effects is difficult in a cross-sectional study; instead, longitudinal studies that follow patients soon after documented HAART initiation are required to confirm the protective effects of HAART on the CNS. These future longitudinal studies should take advantage of advanced longitudinal MRI processing tools to reduce variability and increase statistical power (Aubert-Broche et al., 2013).

Our study applied advanced analytic approaches to assess the effects HIV has on the brain. The study is one of the largest to date of HIV+ individuals typical of those currently followed in specialty clinics in North America and Europe. Most were on stable HAART treatment, and the majority had full viral suppression. VBM and DBM analysis revealed significant volume loss, principally in subcortical and brainstem white matter, and these reductions were associated with nadir CD4+ counts, but not indices of current infection severity. Our results suggest that even currently well-controlled infection has a significant impact on brain volumes. The findings suggest multifactorial etiologies of brain structural differences, with white matter changes, particularly in the brainstem and thalamus, most strongly related to nadir CD4+. The findings provide indirect support for early treatment with HAART to avoid potential long term effects on brain structure and function, although this claim will need to be tested with prospective longitudinal studies.

Chapter 4: Summary

This thesis provided an in-depth overview of the human immunodeficiency virus, magnetic resonance imaging and medical image processing methods. It also reviewed previous MRI studies that have investigated the impact HIV has on the brain. Finally, I provided a manuscript that used deformation-based morphometry and voxel-based morphometry to correlate the regional brain volume changes in an HIV+ cohort against demographically-matched healthy controls, and measures of immune status, and current and past viral suppression.

It is widely known that HIV is a virus that attacks the human immune system. In particular, the CD4+ T-cells are the primary target of the virus. This leads to low CD4+ T-cell counts commonly found in HIV+ patients. With a weak immune response, the body cannot protect itself from life-threatening opportunistic infections and cancers. Thus, before treatment was available, the life expectancy was less than ten years after the initial infection diagnoses (Lima et al., 2007).

Since the discovery of HIV, researchers have successfully learned how the virus replicates, induces CD4+ T cell death, and gains entry into the brain. In particular, this knowledge led to the production of HIV anti-retroviral treatment. Zidovudine or AZT was the first HIV anti-retroviral treatment developed. Although AZT showed promising results in clinical trials, HIV became AZT-resistance after long periods of use. Thus, AZT was not a viable long term treatment option because it was unable to suppress viral replication for longer periods of time and patients ultimately still died (Moore & Chaisson, 1996). In 1996, a new class of anti-retroviral drug was created, namely protease inhibitors, which prevented new viruses from maturing. Investigators then proposed a three-drug HIV therapy that included one protease inhibitor and two NRTIs (Gulick et al., 1997; Hammer et al., 1997). This three-drug therapy, referred to as highly active anti-retroviral therapy, has significantly improved clinical and immune statuses, with a 60-80% decline in rates of AIDS, death and hospitalizations (Moore & Chaisson, 1996). In 2010 alone, it was estimated that HAART saved 700,000 lives around the world (Fauci & Folkers, 2012).

Patients with HIV not only had weak immune responses, but they also experienced HIV-associated neurocognitive disorders (HAND) (Kaul et al., 2001). Although the introduction of HAART has reduced the prevalence of more severe forms of HAND, HIV+ patients continue to show mild to moderate cognitive deficits. In addition, many of these HIV+ individuals still develop cognitive impairment, despite stable HAART treatment, effective viral suppression and good immune recovery.

Many structural MRI studies have examined the pattern and extent of brain injury caused by HIV, but the reported patterns of atrophy are inconsistent across the studies. The inconsistencies likely reflect several factors, including differences in severity of infection in HIV+ cohorts, poorly matched HIV- control group and small sample sizes. In addition, the majority of previous studies employed ROI analysis, which cannot discover unpredicted volume changes, subtle regionally specific volume changes, and when the statistical power is low, null findings may not provide additional information. The results are also dependent on the employed brain structure segmentation method. In the study presented in Chapter 3, DBM and VBM analysis was used to detect structural abnormalities by searching the whole brain simultaneously on a voxel-wise basis, which overcomes the limitations associated with ROI analysis.

The results from the VBM analysis clearly showed significant white matter volume loss in HIV+ patients compared to the control group. White matter atrophy was most pronounced in the brainstem and thalamus, and was independent from the effects of age, gender, ethnicity and education. In contrast, no group differences in gray matter or CSF volumes were detected. Although DBM analysis did not reveal any significant group differences, regional patterns of brain volume loss, similar to VBM, were present at more lenient statistical thresholds. Consistent with our findings, multiple studies have also reported significant volume loss in HIV+ patients in the brainstem and thalamus (Cardenas et al., 2009; Chiang et al., 2007; Janssen et al., 2015; Kallianpur et al., 2013; Küper et al., 2011; Pfefferbaum et al., 2012). These results provide further evidence of brain volume loss among HIV+ individuals in the setting of stable HAART treatment.

Studies have also reported group differences in other basal ganglia structures, such as the caudate (Ances et al., 2012; Becker et al., 2011; Kallianpur et al., 2011), globus pallidus (Chiang et al., 2007), putamen (Becker et al., 2011; Chiang et al., 2007; Kallianpur et al., 2013), amygdala (Ances et al., 2012), hippocampus (Kallianpur et al., 2013) and corpus callosum (Ances et al., 2012; Chiang et al., 2007; Thompson et al., 2006). Although we did not see significant group differences in these subcortical regions, the HIV+ patients in aformentioned studies did not have well-controlled viral replication and many had AIDS-defining illnesses. Together, this suggests that widespread subcortical atrophy most likely occurs in untreated HIV+ individuals with ineffective viral suppression. The apparent proclivity for particular subcortical structures could also be explained by their proximity to the lateral ventricles. This proximity may allow for easier viral penetration by HIV-infected mononuclear cells and HIV toxic products, such as gp120 and

Tat (Ances et al., 2012; Brew, Rosenblum, Cronin, & Price, 1995). In particular, the highest concentrations of HIV have been observed in the corpus callosum and caudate compared to other brain regions (Ances et al., 2012; Brew et al., 1995).

We also assessed the correlation of brain volume measures against nadir CD4+ counts, current CD4+ counts and current viral loads. In HIV+ patients with a history of severe immunosuppression, as indicated by lower nadir CD4+ cell counts, VBM and DBM analysis detected significant white matter atrophy and greater englargement in the third ventricle. In particular, volume loss was most severe in the brainstem, thalamus, caudate, globus pallidus, internal capsule and right frontal lobe, as well as greater enlargement of the third ventricle. These results suggest that early initiation of HAART may be important in protecting long term brain health, and shows that some brain regions are more vulnerable to the effects of HIV-related immunosuppression. The observed correlations corresponds with previous reports, which detected significant atrophy in the brainstem, caudate, and frontal lobe, as well as greater CSF enlargements with lower nadir CD4+ counts (Cardenas et al., 2009; Cohen et al., 2010; Hua et al., 2013; Jernigan et al., 2011).

The study presented in Chapter 3 utilized advanced image processing techniques to assess the impact HIV has on regionally specific brain regions in a large cohort of treated HIV+ patients, with well-controlled viral replication. Compared with a demographically-matched control group, VBM analysis detected significant brain volume loss in subcortical and brainstem white matter. Both DBM and VBM analysis revealed that HIV+ patients with more severe episodes of HIV-related immunosuppression were most vulnerable to brain injury, particularly in the brainstem, thalamus, caudate, globus pallidus, internal capsule and right frontal lobe. Together, our findings suggest that patients with currently well-controlled infection have significant brain volume changes. The results should emphasize the importance of monitoring HIV+ individuals who have had a history of severe immunosuppression, and suggest that early treatment with HAART may avoid long term brain injury.

4.1. Future Work

The manuscript presented in Chapter 3 provided a detail illustration of the nature and extent of brain volume loss in HIV+ patients. Unlike previous studies, we report on a large sample of HIV+ patients, 90% of whom were on stable HAART treatment and the majority had full viral suppression. Our findings suggests that early initiation of HAART treatment may be key to

protecting long term brain health. However, it is difficult to make causal inferences from these results because they are based on cross-sectional analysis. Validation of these results will depend on longitudinal studies tracking the brain volumes relative to measures of immune status, and current and past infection severity in large cohort of HIV+ subjects with structured assessment time points.

Although our sample size was sufficiently large enough to estimate the prevalence of brain injury with adequate precision, extensive inclusion and exclusion criteria were established, and the patient data was collected in contemporaneous manner, it was still difficult to determine the precise cause of brain injury. Our results suggest that multifactorial etiologies of brain structural differences, with white matter changes, particularly in the brainstem and thalamus, most strongly related to nadir CD4+ counts. This could be directly related to the virus prior to treatment initiation, on-going neuroinflammation due to viral reservoirs, or to possible neurotoxic effects of the treatment. To disentangle the precise neuropathology of the infection, large longitudinal studies that follow HIV+ participants soon after documented seroconversion and HAART initiation are required.

It is widely understood that HIV significantly affects a wide variety of subcortical structures. However, regions of the cerebral cortex affected by HIV are not well understood. This may reflect the inability of MRI processing methods to capture subtle cortical volume changes. In particular, ROI analysis is well-suited for detecting changes over a global brain regions, such as total lobar, gray and white matter volumes. Not surprisingly, all previous HIV-related ROI-based studies do not report any significant cortical volume loss due to HIV. Meanwhile, some DBM and VBM studies have detected significant cortical atrophy in the temporal lobe (Becker et al., 2012; Küper et al., 2011) and parietal lobe (Becker et al., 2012). However, these patterns have not been universal since multiple VBM and DBM studies do not observe any significant cortical atrophy (Chiang et al., 2007; Cohen et al., 2010; Hua et al., 2013). The discrepancies between the results may, in part, be explained by the high variability of cortical folding between individuals. Both VBM and DBM are dependent on automated non-linear registration procedures to map each voxel of the individual MRI to its corresponding location on an average brain template. They are thus better-suited to detect subcortical (compared to cortical) volume changes, since subcortical structures show less variability across individuals. The same non-linear registration procedure is

also applied to the cortex, but the wider inter-individual variability in cortical morphology can reduce the statistical power to capture subtle cortical volume changes.

Cortical segmentation and modeling tools provide an alternative, sensitive and quantitative measure of the cortical thickness. Cortical segmentation utilizes the gray and white matter masks, extracted from the patient's MR scan via tissue classification, to fit polygonal meshes onto the white-gray matter boundary (S.F. Eskildsen & Østergaard, 2006). Using gradient vector flow and force balancing schemes, the meshes are inflated towards the pial surface boundary (S.F. Eskildsen & Østergaard, 2006). Cortical thickness is estimated by taking the three-dimensional distance from white-gray matter boundary to the pial surface, and then the thickness maps are blurred along the surface. The extracted cortical surfaces can be aligned with a standard cortical template using non-linear surface-based registration tools. Alignment of homologous cortical regions using non-linear surface registration is more accurate for the cortex than the three-dimensional non-linear registration tools used for VBM and DBM. In particular, Robbins *et al.*, (Robbins, Evans, Collins, & Whitesides, 2004), developed a surface-based registration tool that used depth maps to drive the non-linear registration. The depth maps measured the distance of any point on the cortical surface to a rigid sheet encasing the entire cortex. Vertices on the crowns of gyri have the smallest depth, and vertices in the fundi of sulci have the greatest depth. By aligning homologous cortical regions based on depth maps, the chance of corresponding vertices being in similar positions within a cortical fold is maximized (Robbins et al., 2004). With each cortical thickness vertex in corresponding surface locations, statistical analysis can be performed to produce three-dimensional statistical cortical maps illustrating regions of significant cortical thinning or expansion across study populations.

A study conducted by Thompson *et al.*, (Thompson et al., 2005), utilized cortical modeling to examine the cerebral cortex in AIDS patients. They reported significant cortical thinning in the primary motor and sensory cortex in AIDS patients compared to normal healthy controls. In addition, cortical thinning in the frontopolar and perisylvian language areas were significantly associated with lower current CD4+ counts (Thompson et al., 2005). However, the presented results do not provide an accurate representation of cortical injury in the HAART era because the entire study cohort have had AIDS-defining illnesses. In addition, only 50% of the AIDS patients were currently treated with HAART (Thompson et al., 2005). This suggests that over half of the study's population have not effectively suppressed viral replication. The study also contained a

small sample size with 26 AIDS and 14 control subjects. Future studies investigating the extent of cortical thinning caused by HIV should report on a larger HIV+ cohort, on stable HAART treatment with well-controlled infections. The results of these future studies will provide a better representation of the regionally specific cortical thinning in HIV+ patients in the era of stable treatment.

Deformation-based analysis heavily relies the deformation field that is generated from the non-linear registration procedure. The deformation field contains information about the local brain volume and shape. To recover this information, the Jacobian determinant of the deformation field is computed. Based on the value of this calculation indicates whether there is local brain growth or shrinkage. However, much of the information about the local brain shape is lost when the Jacobian determinant is computed (Lepore et al., 2008). For example, a particular image voxel may have a directional shrinkage and growth (i.e., elongation), but the value of the Jacobian determinant may be close to 1, suggesting that there is no local volume change (Lepore et al., 2008). To overcome this limitation, Lepore *et al.*, (Lepore et al., 2008), developed a multivariate tensor-based morphometry method that recovers the full deformation tensor, such that both local volume and shape changes could be extracted. In the future, HIV-related MRI studies should utilize the multivariate tensor-based morphometry to capture more extensive patterns of structural abnormalities.

The motivation behind this thesis was to characterize the nature and extent of brain injury in HIV+ patients because the prevalence of mild to moderate cognitive impairment appears to be increasing in the HAART era (Ances & Ellis, 2007; Heaton et al., 2011a). In our study, we found significant brain volume changes in HIV+ patients compared to normal healthy controls, as well as changes associated with a history of severe HIV-related immunosuppression. However, we did not investigate the cognitive states of our HIV+ cohort. In future studies, it will be important to examine the cognitive states of HIV+ patients because it will help to compare the results between different studies, since the degree of impairment in an HIV+ cohort could significantly influence the final results. For example, studies with highly impaired HIV+ patients may observe more brain volume loss than a study with cognitively normal HIV+ patients.

Typically, prior HIV studies that examined cognition in HIV+ patients have utilized a standard battery of neuropsychological evaluations, which consists of Trail-Making Tests A & B, the Hopkins Verbal Learning Test-Revised, and the Digit-Symbol Modalities Test (WAIS-III R).

These tests examined memory, psychomotor speed, and executive function and have been previously used to briefly assess cognitive impairment in HIV+ patients (Robertson et al., 2010; VanGorp, Miller, Satz, & Visscher, 1989). To capture the cognitive states from the neuropsychological evaluations, two approaches have been utilized to summarize test performance. The conventional method standardized raw scores from each test using demographic (age, gender, ethnicity and education) adjusted normative means (Heaton et al., 2011b). A Z-score was then calculated by subtracting the appropriate normative mean from the raw score and dividing by the normative standard deviation. The Z-scores from each test were averaged to generate a summary Z-score (NPZ-4). Although widely used in HIV cognitive research, it has been previously shown that the NPZ-4 has several limitations: averaging results in a loss of potentially informative variance, and the resulting score is not a quantity in the strict sense of the word, posing potential difficulties in its use in statistical analyses (Brouillette et al., 2015). An alternative approach, Rasch analysis, avoids these issues (Brouillette et al., 2015). This method, a form of item-response theory, establishes whether the neuropsychological tests fit a single latent construct (i.e. 'cognitive ability'), and if so, produces an estimate of that construct that can be treated as a continuous measure (Brouillette et al., 2015). Rasch is also robust to missing data, which allows it to takes advantage of all available data.

Several studies have reported that subjects with HIV were significantly more cognitively impaired than healthy controls (Ances & Ellis, 2007; Ances et al., 2012; Chiang et al., 2007; Ellis et al., 2007; Küper et al., 2011; Thompson et al., 2006; Thompson et al., 2005), suggesting that brain structural differences relate to brain function. To test for such relationships, future studies should utilize VBM, DBM and cortical modeling to observe the correlation between brain volume measures and neuropsychological test performance. Previous ROI analysis have reported that poorer neuropsychological test performance was significantly associated with smaller caudate and putamen volumes (Becker et al., 2011; Cohen et al., 2010). In contrast, Castelo *et al.*, (Castelo et al., 2007), reported slowed motor performance was significantly associated with enlarged putamen in HIV+ patients. Prior DBM and VBM studies have reported significant atrophy in the corpus callosum, frontal lobe, and primary motor and sensory regions (Chiang et al., 2007), as well as reductions in total gray and white matter volumes, were associated with poorer cognitive scores (Becker et al., 2012). However, the aforementioned studies summarized neuropsychological test scores with the conventional summary Z-score. Future studies should employ the Rasch analysis

because it will provide more variance, and more robust associations, with regional brain volume changes.

4.2. Conclusion

In summary, the goal of this thesis was to investigate and characterize the nature and extent of brain volume changes in HIV+ patients, on stable HAART treatment with effective viral suppression. We observed significant regionally specific volume loss in the brainstem and thalamus in HIV+ patients compared to a demographically similar HIV- comparison group. In addition, patients with previous episodes of more severe immunosuppression had significant atrophy in the brainstem, thalamus, caudate, globus pallidus, internal capsule and right frontal lobe, as well as greater enlargement of the third ventricle. The findings suggest multifactorial etiologies of brain structural differences, with white matter changes, particularly in the brainstem and thalamus, most strongly related to nadir CD4+. The findings provide indirect support for early treatment with HAART to avoid potential long term effects on brain structure.

Although the goal of this thesis was accomplished, the reported findings must be validated with future longitudinal studies that follow HIV+ participants soon after documented seroconversion and HAART initiation. These longitudinal studies will provide greater insight into the precise underlying mechanisms that lead to brain injury and ultimately cognitive impairment.

References

Ances, B. M., & Ellis, R. J. (2007). Dementia and neurocognitive disorders due to HIV-1 infection. *Seminars in Neurology, 27*(1), 86-92. doi: 10.1055/s-2006-956759

Ances, B. M., Orteg, M., Vaida, F., Heaps, J., & Paul, R. (2012). Independent Effects of HIV, Aging and HAART on Brain Volumetric Measures. *Journal of Acquired Immune Deficiency Syndrome, 59*(5), 469-477. doi: 10.1097/QAI.0b013e318249db17.

Antinori, A., Arendt, G., Becker, J. T., Brew, B. J., Byrd, D. A., Cherner, M., . . . Wojna, V. E. (2007). Updated research nosology for HIV-associated neurocognitive disorders. *Neurology, 69*(18), 1789-1799. doi: 10.1212/01.WNL.0000287431.88658.8b.

Ashburner, J., & Friston, K. J. (1999). Nonlinear Spatial Normalization Using Basis Functions. *Human Brain Mapping, 7*, 254-266.

Ashburner, J., & Friston, K. J. (2000). Voxel-Based Morphometry - The Methods. *NeuroImage, 11*(6), 805-821. doi: 10.1006/nimg.2000.0582

Ashburner, J., Hutton, C., Frackowiak, R., Johnsrude, I., Price, C., & Friston, K. J. (1998). Identifying Global Anatomical Differences: Deformation-Based Morphometry *Human Brain Mapping, 6*(5-6), 348-357. doi: 10.1002/(SICI)1097-0193(1998)6:5/6<348::AID-HBM4>3.0.CO;2-P

Aubert-Broche, B., Fonov, V. S., Garcia-Lorenzo, D., Mouiha, A., Guizard, N., Coupé, P., . . . Collins, D. L. (2013). A new method for structural volume analysis of longitudinal brain MRI data and its application in studying the growth trajectories of anatomical brain structures in childhood. *NeuroImage, 82*(15), 393-402. doi: 10.1016/j.neuroimage.2013.05.065

Aylward, E. H., Brettschneider, P. D., McArthur, J. C., Harris, G. J., Schlaepfer, T. E., Henderer, J. D., . . . Pearlson, G. D. (1995). Magnetic resonance imaging measurement of gray matter volume reductions in HIV dementia. *American Journal of Psychiatry, 152*(7), 987-994.

Aylward, E. H., Henderer, J. D., McArthur, J. C., Brettschneider, P. D., Harris, G. J., Barta, P. E., & Pearlson, G. D. (1993). Reduced basal ganglia volume in HIV-1-associated dementia: results from quantitative neuroimaging. *Neurology, 43*(10), 2099-2104.

Bai, Y., Xue, H., Wang, K., Cai, L., Qiu, J., Bi, S., . . . Liu, K. (2013). Covalent fusion inhibitors targeting HIV-1 gp41 deep pocket. *Amino Acids, 44*(2), 701-713.

Baron, J. C., Chétalat, G., Desgranges, B., Perchey, G., Landeau, B., Sayette, V. d. l., & Eustache, F. (2001). *In Vivo* Mapping of Gray Matter Loss with Voxel-Based Morphometry in Mild Alzheimer's Disease. *NeuroImage, 14*(2), 298-309. doi: 10.1006/nimg.2001.0848

Barre-Sinoussi, F., Chermann, J.-C., Rey, F., Nugeyre, M. T., Chamaret, S., Gruest, J., . . . Montagnier, W. R. (1983). Isolation of a T-lymphotropic retrovirus from a patient at risk for acquired immune deficiency syndrome (AIDS). *Science, 220*, 868-871.

Becker, J. T., Maruca, V., Kingsley, L. A., Sanders, J. M., Alger, J. R., Barker, P. B., . . . Selnes, O. (2012). Factors affecting brain structure in men with HIV disease in the post-HAART era. *Neuroradiology, 54*(2), 113-121. doi: 10.1007/s00234-011-0854-2

Becker, J. T., Sanders, J., Madsen, S. K., Ragin, A. B., Kingsley, L., Maruca, V., . . . Thompson, P. M. (2011). Subcortical brain atrophy persists even in HAART-regulated HIV disease. *Brain Imaging Behaviour, 5*(2), 77-85. doi: 10.1007/s11682-011-9113-8.

Bell, J. E. (2004). An update on the neuropathology of HIV in the HAART era. *Histopathology, 45*(6), 549-559. doi: 10.1111/j.1365-2559.2004.02004.x

Beyer, M. K., Janvin, C. C., Larsen, J. P., & Aarsland, D. (2007). A magnetic resonance imaging study of patients with Parkinson's disease with mild cognitive impairment and dementia

using voxel-based morphometry. *Journal of Neurology, Neurosurgery & Psychiatry, 78*(3), 254-259. doi: 10.1136/jnnp.2006.093849

Borghammer, P., Østergaard, K., Cumming, P., Gjedde, A., Rodell, A., Hall, N., & Chakravarty, M. M. (2010). A deformation-based morphometry study of patients with early-stage Parkinson's disease. *European Journal of Neurology, 17*(2), 314-320. doi: 10.1111/j.1468-1331.2009.02807.x.

Brew, B. J., Rosenblum, M., Cronin, K., & Price, R. W. (1995). AIDS dementia complex and HIV-1 brain infection: clinical-virological correlations. *Annals of Neurology, 38*(4), 563-570.

Brouillette, M., Mayo, N., Fellows, L. K., Lebedeva, E., Higgins, J., Overton, E. T., . . . Koski, L. (2015). A better screening tool for HIV-associative neurocognitive disorders: is it what clinicians need? *AIDS, 29*, 895-902.

Brummer, M. E. (1992). Optimized intensity thresholds for volumetric analysis of magnetic resonance imaging data. *Proc. SPIE, 1808*, 299-310.

Camicioli, R., Moore, M. M., Kinney, A., Corbridge, E., Glassberg, K., & Kaye, J. A. (2003). Parkinson's disease is associated with hippocampal atrophy. *Movement Disorders, 18*(7), 784-790.

Cardenas, V. A., Meyerhoff, D. J., Studholme, C., Kornak, J., Rothlind, J., Lampiris, H., . . . Weiner, M. W. (2009). Evidence for ongoing brain injury in human immunodeficiency virus-positive patients treated with antiretroviral therapy. *Journal of NeuroVirology, 15*(4), 324-333. doi: 10.1080/13550280902973960

Castelo, J. M. B., Courtney, M. G., Melrose, R. J., & Stern, C. E. (2007). Putamen Hypertrophy in Nondemented Patients With Human Immunodeficiency Virus Infection and Cognitive Compromise. *Archives of Neurology, 64*(9), 1275-1280.

Chanh, T. C., Kennedy, R. C., & Kanda, P. (1988). Synthetic peptides homologous to HIV transmembrane glycoprotein suppress normal human lympocyte blastogenic response. *Cellular Immunology, 111*, 77-86.

Chiang, M., Dutton, R. A., Hayashi, K. M., Lopez, O. L., Aizenstein, H. J., Toga, A. W., . . . Thompson, P. M. (2007). 3D pattern of brain atrophy in HIV/AIDS visualized using tensor-based morphometry. *NeuroImage, 34*(1), 44-60. doi: 10.1016/j.neuroimage.2006.08.030

Chung, M. K., Worsley, K. J., Paus, T., Cherif, C., Collins, D. L., Giedd, J. N., . . . Evans, A. C. (2001). A Unified Statistical Approach to Deformation-Based Morphometry. *NeuroImage, 14*(3), 595-606. doi: 10.1006/nimg.2001.0862

Coffin, J. M. (1992). Superantigens and endogenous retroviruses: a confluence of puzzles. *Science, 255*, 411-413.

Cohen, R. A., Harezlak, J., Schifitto, G., Hana, G., Clark, U., Gongvatana, A., . . . Navia, B. (2010). Effects of NadirCD4 Count and Duration of HIV Infection on Brain Volumes in the HAART Era. *Journal of NeuroVirology, 16*(1), 25-32. doi: 10.3109/13550280903552420

Collins, D. L., Holmes, C. J., Peters, T. M., & Evans, A. C. (1995). Automatic 3-D Model-Based Neuroanatomical Segmentation. *Human Brain Mapping, 3*(3), 190-208. doi: 10.1002/hbm.460030304

Collins, D. L., Neelin, P., Peters, T. M., & Evans, A. C. (1994). Automatic 3D intersubject registration of MR volumetric data in standardized Talairach space. *Journal of Computed Assisted Tomography, 18*(2), 192-205.

Csernansky, J. G., Wang, L., Swank, J., Miller, J. P., Gado, M., McKeel, D., . . . Morris, J. C. (2005). Preclinical detection of Alzheimer's disease: hippocampal shape and volume predict dementia onset in the elderly. *NeuroImage, 25*(3), 783-792.

Das, K., & Arnold, E. (2013). HIV-1 reverse transcriptase and antiviral drug resistance. Part 1. *Current Opinion in Virology, 3*(2), 111-118.

Dewey, J., Hana, G., Russell, T., Price, J., McCaffrey, D., Harezlak, J., . . . Tate, D. F. (2010). Reliability and validity of MRI-based automated volumetry software relative to auto-assisted manual measurement of subcortical structures in HIV-infected patients from a multisite study. *NeuroImage, 51*(4), 1334-1344. doi: 10.1016/j.neuroimage.2010.03.033.

Ellis, R. J., Badiee, J., Vaida, F., Letendre, S., Heaton, R. K., Clifford, D., . . . Grant, I. (2011). CD4 nadir is a predictor of HIV neurocognitive impairment in the era of combination antiretroviral therapy. *AIDS, 25*(14).

Ellis, R. J., Langford, D., & Masliah, E. (2007). HIV and antiretroviral therapy in the brain: neuronal injury and repair. *Nature Reviews Neuroscience, 8*(1), 33-44. doi: 10.1038/nrn2040

Eskildsen, S. F., Coupe, P., Fonov, V., Manjon, J. V., Leung, K. K., Guizard, N., . . . Collins, D. L. (2012). BEaST: Brain Extraction based on nonlocal Segmentation Technique. *NeuroImage, 59*(3), 2362–2373.

Eskildsen, S. F., & Østergaard, L. R. (2006). *Active Surface Approach for Extraction of the Human Cerebral Cortex from MRI.* Paper presented at the Medical Image Computing and Computer-Assisted Intervention.

Fauci, A. S., & Folkers, G. K. (2012). Towards an AIDS-Free Generation. *The Journal of the American Medical Association, 308*(4), 343-344.

Fischl, B., Salat, D. H., Busa, E., Albert, M., Dieterich, M., Haselgrove, C., . . . Dale, A. M. (2002). Whole Brain Segmentation: Automated Labelling of Neuroanatomical Strucutures in the Human Brain. *Neurotechnique, 33*, 341-355.

Folks, T. M., Kessler, S. W., Orenstein, J. M., Justment, J. S., Jaffe, E. S., & Fauci, A. S. (1988). Infection and replication of HIV-1 in purified progenitor cells of normal human bone marrow. *Science, 242*, 919-922.

Fonov, V. S. (2009). ICBM 152 Nonlinear atlases version 2009. from http://www.bic.mni.mcgill.ca/ServicesAtlases/ICBM152NLin2009

Fonov, V. S., Evans, A. C., McKinstry, R. C., Almli, C. R., & Collins, D. L. (2009). Unbiased nonlinear average age-appropriate brain templates from birth to adulthood. *NeuroImage, 47*(1), S102.

Genovese, C. R., Lazar, N. A., & Nichols, T. (2002). Thresholding of Statistical Maps in Functional Neuroimaging Using the False Discovery Rate. *NeuroImage, 15*(4), 870-878. doi: 10.1006/nimg.2001.1037

Good, C. D., Johnsrude, I. S., Ashburner, J., Henson, R. N., Friston, K. J., & Frackowiak, R. S. (2001). A Voxel-Based Morphometric Study of Ageing in 465 Normal Adult Human Brains. *NeuroImage, 14*(1), 21-36. doi: 10.1006/nimg.2001.0786

Gray, F., Scaravalli, F., Everall, I., Chretien, F., An, S., Boche, D., . . . Lantos, P. (1996). Neuropathology of Early HIV-1 Infection. *Brain Pathology, 6*(1), 1-12.

Gulick, R. M., Mellors, J. W., Havlir, D., Eron, J. J., Gonzalez, C., McMahon, D., . . . Condra, J. H. (1997). Treate with Indinavir, Zidovudine, and Lamivudine in Adults with Human Immunodeficiency Virus Infection and Prior Antiretroviral Therapy. *The New England Journal of Medicine, 337*, 734-739.

Hammer, S. M., Squires, K. E., Hughes, M. D., Grimes, J. M., Demeter, L. M., Currier, J. S., . . . Cook, J. C. (1997). A Controlled Trial of Two Nucleoside Analogues plus Indinavir in

Persons with Human Immunodeficiency Virus Infection and CD4 Cell Counts of 200 per Cubic Millimeter or Less. *The New England Journal of Medicine, 337*, 725-733.

Heaton, R. K., Franklin, D. R., Ellis, R. J., McCutchan, J. A., Letendre, S. L., LeBlanc, S., . . . Grant, I. (2011a). HIV-associated neurocognitive disorders before and during the era of combination antiretroviral therapy: Differences in rates, nature and predictors. *Journal of NeuroVirology, 17*(1), 3-16. doi: 10.1007/s13365-010-0006-1.

Heaton, R. K., Franklin, D. R., Ellis, R. J., McCutchan, J. A., Letendre, S. L., Leblanc, S., . . . Grant, I. (2011b). HIV-associated neurocognitive disorders before and during the era of combination antiretroviral therapy: differences in rates, nature, and predictors. *Journal of NeuroVirology, 17*(1), 3-16.

Heindel, W. C., Jernigan, T. L., Archibald, S. L., Achim, C. L., Masliah, E., & Wiley, C. A. (1994). The relationship of quantitative brain magnetic resoance imaging measures to neuropathic index of human immunodeficiency virus infection. *Archives of Neurology, 51*(11), 1129-1135.

Hesselgesser, J., Halks-Miller, M., DelVecchio, V., Peiper, S. C., Hoxie, J., Kolson, D. L., . . . Horuk, R. (1997). CD4-independent association between HIV-1 gp120 and CXCR4: functional chemokine receptors are expressed in human neurons. *Current Biology, 7*(2), 112-121.

. *HIV Virus Replication Cycle*. (2010).

Holt, J. L., Kraft-Terry, S. D., & Chang, L. (2012). Neuroimaging studies of the aging HIV-1-infected brain. *Journal of NeuroVirology, 18*(4), 291-302. doi: 10.1007/s13365-012-0114-1

Hua, X., Boyle, C. P., Harezlak, J., Tate, D. F., Yiannoutsos, C. T., Cohen, R., . . . Thompson, P. M. (2013). Disrupted cerebral metabolite levels and lower nadir CD4+ counts are linked to brain volume deficits in 210 HIV-infected patients on stable treatment. *NeuroImage: Clinical, 3*, 132-142. doi: 10.1016/j.nicl.2013.07.009

Hua, X., Leow, A. D., Parikshak, N., Lee, S., Chiang, M., Toga, A. W., . . . Thompson, P. M. (2008). Tensor-based morphometry as a neuroimaging biomarker for Alzheimer's disease: An MRI study of 676 AD, MCI, and normal subjects. *NeuroImage, 43*(3), 458-469. doi: 10.1016/j.neuroimage.2008.07.013

Janssen, M. A. M., Meulenbroek, O., Steens, S. C. A., Goraj, B., Bosch, M., Koopmans, P. P., & Kessels, R. P. C. (2015). Cognitive function, wellbeing and brain correlates in HIV-1 infected patients on long-term combination antiretroviral therapy. *AIDS, 29*, 2139-2148. doi: 10.1097/QAD.0000000000000824

Jernigan, T. L., Archibald, S., Hesselink, J. R., Atkinson, J. H., Velin, R. A., McCutchan, J. A., . . . Grant, I. (1993). Magnetic resonance imaging morphometric analysis of cerebral volume loss in human immunodeficiency virus infection. *Archives of Neurology, 50*, 250-255.

Jernigan, T. L., Archibald, S. L., Fennema-Notestine, C., Taylor, M. J., Theilmann, R. J., Julaton, M. D., . . . Grant, I. (2011). Clinical factors related to brain structure in HIV: the CHARTER study. *Journal of NeuroVirology, 17*(3), 248-257. doi: 10.1007/s13365-011-0032-7

Kallianpur, K. J., Kirk, G. R., Sailasuta, N., Valcour, V., Shiramizu, B., Nakamoto, B. N., & Shikuma, C. (2011). Regional Cortical Thinning Associated with Detectable Levels of HIV DNA. *Cerebral Cortex, 22*(9), 2065-2075. doi: 10.1093/cercor/bhr285

Kallianpur, K. J., Shikuma, C., Kirk, G. R., Shiramizu, B., Valcour, V., Chow, D., . . . Sailasuta, N. (2013). Peripheral blood HIV DNA is associated with atrophy of cerebellar and

subcortical gray matter. *Neurology, 80*(19), 1792-1799. doi: 10.1212/WNL.0b013e318291903f

Kaul, M., Garden, G. A., & Lipton, S. A. (2001). Pathways to neuronal injury and apoptosis in HIV-associated dementia. *Nature, 410*, 988-994.

Kaul, M., & Lipton, S. (1999). Chemokines and activated macrophages in HIV gp120-induced neuronal apoptosis. *Proceedings of the National Academy of Sciences of the United States of America, 96*, 8212-8216.

Klein, A., Andersson, J., Ardekani, B. A., Ashburner, J., Avants, B., Chiang, M., . . . Parsey, R. V. (2009). Evaluation of 14 nonlinear deformation algorithms applied to human brain MRI registration. *NeuroImage, 46*(3), 786-802.

Kundu, A. (1990). Local segmentation of biomedical images. *Comput. Med. Imag. Graph., 14*, 173-183.

Küper, M., Rabe, K., Esser, S., Gizewski, E. R., Husstedt, I. W., Maschke, M., & Obermann, M. (2011). Structural gray and white matter changes in patients with HIV. *Journal of Neurology, 258*(6), 1066-1075. doi: 10.1007/s00415-010-5883-y

Lambotte, O., Deiva, K., & Tardieu, M. (2003). HIV-1 Persistence, Viral Reservoir, and the Central Nervous System in the HAART era. *Brain Pathology, 13*, 95-103.

Lanzavecchia, A., Roosnek, E., Gregory, T., Berman, P., & Abrignani, S. (1988). T cells can present antigens such as HIV gp120 targeted to their own surface molecules. *Nature, 334*, 530-532.

Lawrence, D. M., & Major, E. O. (2002). HIV-1 and the brain: connections between HIV-1-associated dementia, neuropathology and neuroimmunology. *Microbes and Infection, 4*(3), 301-308. doi: 10.1016/S1286-4579(02)01542-3

Lepore, N., Brun, C., Chou, Y., Chiang, M., Dutton, R. A., Hayashi, K. M., . . . Thompson, P. M. (2008). Generalized Tensor-Based Morphometry of HIV/AIDS Using Multivariate Statistics on Deformation Tensors. *IEEE Transactions on Medical Imaging, 27*(1), 129-141.

Levy, J. A. (1993). Pathogensis of human immunodeficiency virus infection. *Microbiological Reviews, 57*(1), 183-289.

Lieberman-Blum, S. S., Fung, H. B., & Bandres, J. C. (2008). Maraviroc: A CCR5-Receptor Antagonist for the Treatment of HIV-1 Infection. *Clinical Therapeutics, 30*(7), 1228-1250.

Lima, V. D., Hogg, R. S., Harrigan, P. R., Moore, D., Yip, B., Wood, E., & Montaner, J. S. (2007). Continued improvement in survival among HIV-infected individuals with newer forms of highly active antiretroviral therapy. *AIDS, 21*(6), 685-692.

Lipton, S., & Gendelman, H. E. (1995). Dementia associated with the acquired immunodeficiency syndrome. *The New England Journal of Medicine, 43*, 2245-2252.

Markowitz, M., Saag, M., Powerdly, W. G., Hurley, A. M., Hsu, A., Valdes, J. M., . . . Ho, D. D. (1995). A Preliminary Study Ritonavir, an Inhibitor of HIV-1 Protease, to Treat HIV-1 Infection. *The New England Journal of Medicine, 333*, 1534-1540.

Masters, M. C., & Ances, B. M. (2014). Role of Neuroimaging in HIV Associated Neurocognitive Disorders (HAND). *Seminars in Neurology, 34*(1), 89-102. doi: 10.1055/s-0034-1372346

McArthur, J. C., Hoover, D. R., Bacellar, H., Miller, E. N., Cohen, B. A., Becker, J. T., . . . Saah, A. (1993). Dementia in AIDS patients. *Neurology, 43*(11).

Merson, M. H. (2006). The HIV–AIDS Pandemic at 25 — The Global Response. *The New England Journal of Medicine, 354*, 2414-2417.

Metifiot, M., Marchand, C., & Pommier, Y. (2013). HIV Integrase Inhibitors: 20-Year Landmark and Challenges. *Advances in Pharmacology, 67*, 75-101.

Meucci, O., Fatatis, A., Simen, A. A., Bushell, T. J., Gray, P. W., & Miller, R. J. (1998). Chemokines regulate hippocampal neuronal signaling and gp120 neurotoxicity. *Proceedings of the National Academy of Sciences of the United States of America, 95*(24), 14500-14505.

Mitsuya, H., Weinhold, K. J., Furman, P. A., Clair, M. H. S., Lehrmen, S. N., Gallo, R. C., . . . Broder, S. (1985). 3'-Azido-3'-deoxythymidine (BW A509U): an antiviral agent that inhibits the infectivity and cytopathic effect of human T-lymphotropic virus type III/lymphadenopathy-associated virus in vitro. *Proceedings of the National Academy of Sciences of the United States of America, 82*(20), 7096-7100.

Molotsky, I. (1987, March 21, 1987). U.S. Approves Drug to Prolong Lives in AIDS Patients. *New York Times*.

Moore, R. D., & Chaisson, R. E. (1996). Natural History of Opportunistic Disease in an HIV-Infected Urban Clinical Cohort. *Annals of Internal Medicine, 124*(7), 633-642.

Pfefferbaum, A., Rosenbloom, M. J., Sassoon, S. A., Kemper, C. A., Deresinki, S., Rohlfing, T., & Sullivan, E. V. (2012). Regional Brain Structural Dysmorphology in HIV Infection: Effects of AIDS, Alcoholism, and Age. *Biological Psychiatry, 72*(5), 361-370.

Pluim, J. P. W., Maintz, J. B. A., & Viergever, M. A. (2000). Image Registration by Maximization of Combined Mutual Information and Gradient Information. *Medical Image Computing and Computer-Assisted Intervention, 1935*, 452-461.

Ragin, A. B., Du, H., Ochs, R., Wu, Y., Sammet, C. L., Shoukry, A., & Epstein, L. G. (2012). Structural brain alterations can be detected early in HIV infection. *Neurology, 79*(24), 2328-2334. doi: 10.1212/WNL.0b013e318278b5b4

The replication cycle of HIV. (2000). from http://www.biology.arizona.edu/immunology/tutorials/aids/treatment.html

Robbins, S., Evans, A. C., Collins, D. L., & Whitesides, S. (2004). Tuning and comparing spatial normalization methods. *Medical Image Analysis, 8*(3), 311-323.

Robertson, K. R., Su, Z., Margolis, D. M., Krambrink, A., Havlir, D. V., Evans, S., & Skiest, D. J. (2010). Neurocognitive effects of treatment interruption in stable HIV-positive patients in an observational cohort. *Neurology, 74*(16), 1260-1266. doi: 10.1212/WNL.0b013e3181d9ed09.

Schouten, J., Cinque, P., Gisslen, M., Reiss, P., & Portegies, P. (2011). HIV-1 infection and cognitive impairment in the cART era: A review. *AIDS, 25*(3), 561-575. doi: 10.1097/QAD.0b013e3283437f9a.

Selik, R. M., Mokotoff, E. D., Branson, B., Owen, S. M., Whitmore, S., & Hall, H. I. (2014). *Revised Surveillance Case Definition for HIV Infection*.

Simioni, S., Cavassini, M., Annoni, J. M., Abraham, A. R., Bourquin, I., Schiffer, V., . . . Pasquier, R. A. D. (2010). Cognitive dysfunction in HIV patients despite long-standing suppression of viremia. *AIDS, 24*(9), 1243-1250. doi: 10.1097/QAD.0b013e3283354a7b.

Sled, J. G., Zijdenbos, A. P., & Evans, A. C. (1998). A nonparametric method for automatic correction of intensity nonuniformity in MRI data. *IEEE Transactions on Medical Imaging, 17*(1), 87-97. doi: 10.1109/42.668698

Stevenson, M., Meier, C., Mann, A. M., Chapman, N., & Wasiak, A. (1988). Envelope glycoprotein of HIV induces interference and cytolosis resistance in CD4+ cells: mechanism for persistence in AIDS. *Cell, 53*, 483-496.

Stout, J. C., Ellis, R. J., Jernigan, T. L., Archibald, S. L., Abramson, I., Wolfson, T., . . . Grant, I. (1998). Progressive cerebral volume loss in human immunodeficiency virus infection: a longitudinal volumetric magnetic resonance imaging study. HIV Neurobehavioral Research Center Group. *Archives of Neurology, 55*(2), 161-168. doi: 10.1001/archneur.55.2.161.

Talairach, J., & Tournoux, P. (1988). *Co-Planar Stereotaxic Atlas of the Human Brain: 3-Dimensional Proportional System - An Approach to Cerebral Imagin*. New York: Thieme Medical Publishers.

Thompson, P. M., Dutton, R. A., Hayashi, K. M., Lu, A., Lee, S. E., Lee, J. Y., . . . Becker, J. T. (2006). 3D mapping of ventricular and corpus callosum abnormalities in HIV/AIDS. *NeuroImage, 31*(1), 12-23. doi: 10.1016/j.neuroimage.2005.11.043

Thompson, P. M., Dutton, R. A., Hayashi, K. M., Toga, A. W., Lopez, O. L., Aizenstein, H. J., & Becker, J. T. (2005). Thinning of the cerebral cortex visualized in HIV/AIDS reflects CD4+ T lymphocyte decline. *Proceedings of the National Academy of Sciences of the United States of America, 102*(43), 15647-15652. doi: 10.1073/pnas.0502548102

Thompson, P. M., & Toga, A. W. (1999). Anatomically driven strategies for high-dimensional brain image warping and pathology detection. *Brain Warping, 311-336*.

Tustison, N., & Gee, J. (2009). N4ITK: Nick's N3 ITK Implementation For MRI Bias Field Correction. *The Insight Journal, 2009 January - June*.

VanGorp, W. G., Miller, E. N., Satz, P., & Visscher, B. (1989). Neuropsychological performance in HIV-1 immunocompromised patients: a preliminary report. *Journal of Clinical and Experimental Neuropsychology, 11*(5), 763-773. doi: 10.1080/01688638908400930

Viscidi, R. P., Mayur, K., Lederman, H. M., & Frankel, A. D. (1989). Inhibition of antigen-induced lymphocte proliferation by *tat* protein from HIV-1. *Science, 246*, 1606-1608.

Wang, K. (2014). Dragging HIV into the Limelight: Exposing the Anatomy of the World's Leading Infectious Killer. *Yale Scientific.* from http://www.yalescientific.org/2014/12/dragging-hiv-into-the-limelight-exposing-the-anatomy-of-the-worlds-leading-infectious-killer/

Wells, W. M., Grimson, E. L., Kikinis, R., & Jolesz, F. A. (1996a). Adaptive segmentation of MRI data. *IEEE Transactions on Medical Imaging, 15*, 429-442.

Wells, W. M., Grimson, W. E. L., Kikinis, R., & Jolesz, F. A. (1996b). Adaptive Segmentation of MRI Data. *IEEE Transactions on Medical Imaging, 15*(4).

Worsley, K. J., Andermann, M., Koulis, T., MacDonald, D., & Evans, A. C. (1999). Detecting changes in non-isotropic images. *Human Brain Mapping, 9*, 98-101.

Wright, K. (1986). First tentative signs of theraputic promise. *Nature, 323*, 283.

Zhang, Y., Brady, M., & Smith, S. (2001). Segmentation of Brain MR Images Through a Hidden Markov Random Field Model and the Expectation-Maximization Algorithm. *IEEE Transactions on Medical Imaging, 20*(1), 45-58.

Zijdenbos, A. P., Forghani, R., & Evans, A. C. (2002). Automatic 'pipeline' analysis of 3-D MRI data for clinical trials: application to multiple sclerosis. *IEEE Transactions on Medical Imaging, 21*(10), 1280-1291. doi: 10.1109/TMI.2002.806283